NUREG/CR-0766
HEDL-TME 79-3
RT

MASTER

DYNAMIC ANALYSIS TO ESTABLISH NORMAL SHOCK AND VIBRATION OF RADIOACTIVE MATERIAL SHIPPING PACKAGES

QUARTERLY PROGRESS REPORT
OCTOBER 1, 1978 - DECEMBER 31, 1978

Hanford Engineering Development Laboratory

HANFORD ENGINEERING DEVELOPMENT LABORATORY
Operated by Westinghouse Hanford Company
P.O. Box 1970 Richland, WA 99352
A Subsidiary of Westinghouse Electric Corporation
Prepared for the U.S. Nuclear Regulatory Commission
under Interagency Agreement DOE EY-76-C-14-2170
NRC FIN No. B2263

Available from
National Technical Information Service
Springfield, Virginia 22161

DISCLAIMER

NUREG/CR-0766
HEDL-TME 79-3
RT

DYNAMIC ANALYSIS TO ESTABLISH NORMAL SHOCK AND VIBRATION OF RADIOACTIVE MATERIAL SHIPPING PACKAGES

QUARTERLY PROGRESS REPORT
OCTOBER 1, 1978 - DECEMBER 31, 1978

Hanford Engineering Development Laboratory

S. R. Fields
S. J. Mech

June 1979

HANFORD ENGINEERING DEVELOPMENT LABORATORY
Operated by Westinghouse Hanford Company
P.O. Box 1970 Richland, WA 99352
A Subsidiary of Westinghouse Electric Corporation
Prepared for the U.S. Nuclear Regulatory Commission
under Interagency Agreement DOE EY-76-C-14-2170
NRC FIN No. B2263

NUREG/CR-0766
HEDL-TME 79-3
RT

DYNAMIC ANALYSIS TO ESTABLISH NORMAL SHOCK AND VIBRATION OF RADIOACTIVE MATERIAL SHIPPING PACKAGES

Quarterly Progress Report
October 1, 1978 - December 31, 1978

S. R. Fields
S. J. Mech

ABSTRACT

This report presents work performed at the Hanford Engineering Development Laboratory operated by Westinghouse Hanford Company, a subsidiary of Westinghouse Electric Corporation, for the Nuclear Regulatory Commission, under Department of Energy Contract No. EY-76-C-14-2170. It describes technical progress made during the reporting period by Westinghouse Hanford Company and supporting contractors.

CONTENTS

FIGURES

FIGURES (Cont'd)

TABLES

DYNAMIC ANALYSIS TO ESTABLISH NORMAL SHOCK AND VIBRATION OF RADIOACTIVE MATERIAL SHIPPING PACKAGES

Quarterly Progress Report
October 1, 1978 - December 31, 1978

I. SUMMARY OF PROGRESS

A. DEVELOP DYNAMIC MODEL (TASK 1)

The basic radioactive material shipping cask-rail car dynamic simulator model, CARDS, has been modified to incorporate the following latest developments:

1) Draft gear submodels were installed for the couplers between cars,

2) Suspension subsystem submodels were installed at the front and rear trucks of the cask-rail car,

3) A term defining the vertical friction force at the coupler face was added to the equations of motion for the cask-rail car, and

4) The model was expanded to include equations of motion for each car in an "anvil" train.

Upon completion of the above modifications, a simulation run was made to test the improved version of CARDS. Calculated results show how the shock of impact is propagated through the train. These are presented as plots of coupler force between cars, horizontal displacement of each car in the train, and vertical displacements of points on the cask-rail car, as functions of time after impact.

A subroutine was developed for the CARDS model to convert the displacement, velocity and acceleration response of a cask-rail car system from the time domain to the frequency domain. This subroutine will allow the response spectra to be determined directly from either model output or from test data.

B. DATA COLLECTION AND REDUCTION (TASK 2)

Some of the data recorded during the rail car impact tests conducted at the Savannah River Laboratories from July 14, 1978 through August 3, 1978 have been reduced and analyzed. The reduced data were from Test 1 and were limited to the outputs from Instruments 4, 8 through 12, and 22. Test 1 was an 8.3-mph impact of a 70-ton Seaboard Coastline (SCL) rail car with a standard coupler, carrying a 40-ton Hallam cask held in place by bolted tiedowns with stops. Results of the reduction of these limited data are presented as plots of horizontal and vertical acceleration as functions of time, horizontal displacement as a function of time, horizontal and vertical accelerations as functions of frequency, and transfer function magnitudes as functions of frequency.

II. INTRODUCTION

This study was initiated in October 1977 as stated earlier in previous Quarterly Progress Reports. The objective of this study is to determine the extent to which the shocks and vibrations experienced by radioactive material shipping packages during normal transport conditions are influenced by, or are sensitive to, various structural parameters of the transport system (i.e., package, package supports, and vehicle). The purpose of this effort is to identify those parameters which significantly affect the normal shock and vibration environments so as to provide the basis for determining the forces transmitted to radioactive material packages. Determination of these forces will provide the input data necessary for a broad range of package-tiedown structural assessments.

This is the fifth Quarterly Progress Report on this work. The study consists of seven tasks. Progress on these tasks during this reporting period will now be discussed.

III. PROGRESS TO DATE

The work plan for this study has been revised and is currently under review. The tasks, as established in previous progress reports, have remained the same, but the scheduling has changed. A discussion of progress on each of these tasks during this reporting period will now be presented.

A. DEVELOP DYNAMIC MODEL (TASK 1)

Although the basic radioactive material shipping cask-rail car dynamic simulator model, CARDS, has been established, new features are continually being added and modifications made to make it a better tool for simulation of "real world" conditions. Additions and modifications made during this quarter include:

1) Draft gear submodels were installed for the couplers between cars,
2) Suspension subsystem submodels were installed at the front and rear trucks of the cask-rail car,
3) A term defining the vertical friction force at the coupler face was added to the equations of motion for the cask-rail car,
4) The model was expanded to include equations of motion for each car in an "anvil" train.

The development of the draft gear submodels installed is described in detail in the previous Quarterly Progress Report.[1] This same approach was used to develop a suspension subsystem submodel.

Like the coupler subsystem, suspension subsystems consist of springs and dampers in parallel, as illustrated in Figure 1. In a Barber stabilized truck,[2] the stabilizing or damping friction force is proportional to the load on the truck. Therefore the spring constants for the equivalent springs shown in Figure 1 are defined by equations similar to those for the draft gears, i.e.,

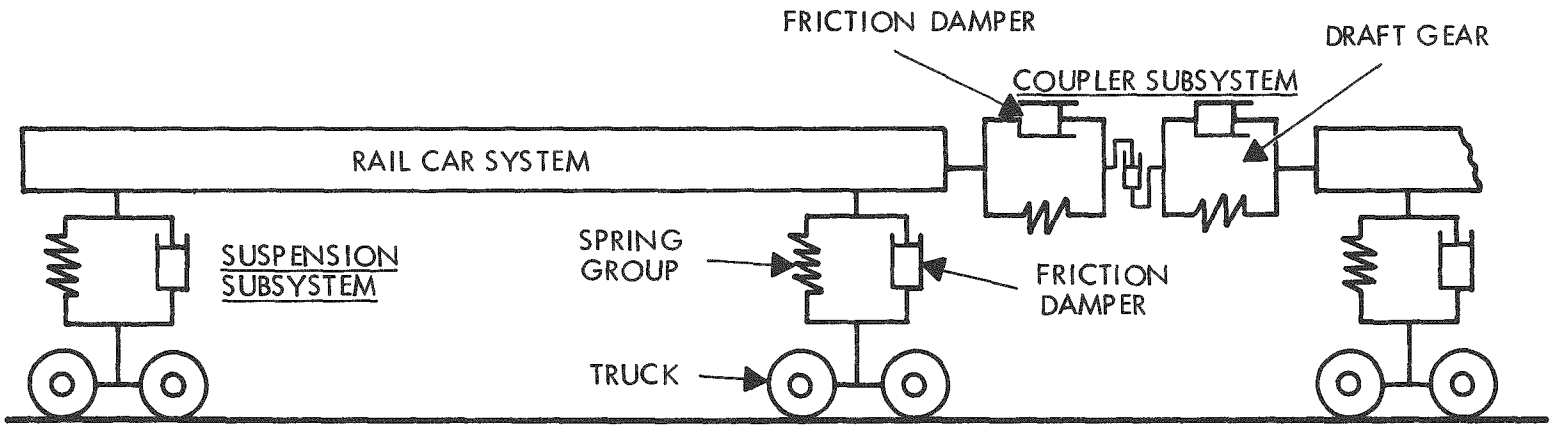

FIGURE 1. Arrangement of Springs and Dampers Simulating Rail Car Coupler and Suspension Subsystems. Neg 7904699-1

$$k_{S6} = k_6\left[1 - \mu_{D6}\beta_6 \operatorname{sgn}\left(\dot{Y}_{RC56}\right)\right] \qquad Y_{RC56} > Y_{RCMAX} \qquad (1)$$

or

$$k_{S6} = k_{6S} \qquad Y_{RC56} \leq Y_{RCMAX} \qquad (2)$$

and

$$k_{S7} = k_7\left[1 - \mu_{D7}\beta_7 \operatorname{sgn}\left(\dot{Y}_{RC78}\right)\right] \qquad Y_{RC78} > Y_{RCMAX} \qquad (3)$$

or

$$k_{S7} = k_{7S} \qquad Y_{RC78} \leq Y_{RCMAX} \qquad (4)$$

where

k_{S6}, k_{S7} = the spring constants for the equivalent springs representing the rear and front suspensions, respectively, lb (force)/inch

K_6, k_7 = the spring constants of the combined springs in the rear and front suspensions, respectively, in their "active" state, lb (force)/inch

k_{6S}, k_{7S} = the spring constants of the combined springs in the rear and front suspensions, respectively, in their "solid" state, i.e., after they have bottomed out, lb (force)/inch

$\dot{Y}_{RC56}, \dot{Y}_{RC78}$ = the vertical displacement velocities of the rail car at the rear and front suspensions, respectively, in./sec

Y_{RCMAX} = the maximum downward vertical displacement of the rail car (the point at which the suspension springs bottom out or go "solid"), inches

Y_{RC56}, Y_{RC78} = the vertical displacements of the rail car at the rear and front suspensions, respectively, inches

μ_{D6}, μ_{D7} = multiplying factors corresponding to coefficients of friction for the dampers in the rear and front suspensions, respectively.

β_6, β_7 = multiplying factors representing the fraction of the load on the respective suspensions which is applied perpendicular to the sliding surfaces of the damper,

and

$\text{sgn}\left(\dot{Y}_{RC56}\right)$, $\text{sgn}\left(\dot{Y}_{RC78}\right)$ = the signum functions or sign functions of $\dot{Y}_{RC56}$ and $\dot{Y}_{RC78}$, respectively.

The signum function is defined as follows for an argument $\dot{Y}$

$$\text{sgn}\ (\dot{Y}) = \begin{cases} +1 & , \quad \dot{Y} > 0 \\ 0 & , \quad \dot{Y} = 0 \\ -1 & , \quad \dot{Y} < 0 \end{cases} \tag{5}$$

Equations (1) and (3) differ from those of the draft gears in two ways. First, the sign of the second term is opposite to that of the draft gear equations. This is necessary since the sign convention used for the model is positive horizontal displacement to the right and positive vertical displacement upward. With this convention, the velocity of the vertical displacement is negative downward in the direction of the load compressing the suspension subsystem. A negative value of this velocity in Equations (1) and (3) will result in the addition of the terms in the brackets. The net result is that the equivalent springs for the suspension subsystems will be stiffer during compression than during relaxation or lifting. The second way in which Equations (1) and (3) differ from those of the draft gears is due to the multiplying factors β_6 and β_7. These factors are related to the action of the so-called "side springs" which apply the force perpendicular to the sliding surfaces of the damping device. These factors represent fractions of the force on the respective suspension subsystems which are actually applied to the sliding surfaces for damping.

When the cask-rail car strikes one or more anvil cars, it will tend to rotate about its center of gravity such that the striking or front end will tend to move downward and the far or rear end will move upward. This rotational or pitching motion is opposed by the damping in the suspension

subsystems, and by frictional damping due to the vertical sliding motion of the coupler face on the cask-rail car against the coupler face on the adjacent anvil car. This frictional force at the coupler faces is represented as a vertical dashpot in Figure 1.

The energy dissipated as frictional work at the coupler faces was defined as

$$W_{CRF} = F_{YRF} Y_{CPL} \tag{6}$$

where

W_{CRF} = the energy dissipated as frictional work, lb (force)-inch,

F_{YRF} = the frictional force opposing the movement of the sliding coupler faces, lb (force)

Y_{CPL} = the vertical displacement of the coupler face on the cask-rail car, inches

The frictional force F_{YRF} was defined by the expression

$$F_{YRF} = -\mu_{CPL} \left| F_{CPL} \right| \text{sgn} (\dot{Y}_{CPL}) \beta_{CPL} \tag{7}$$

$\left| F_{CPL} \right|$ = the absolute value of the force applied to the coupler faces, perpendicular to the sliding surfaces, lb (force)

$\dot{Y}_{CPL}$ = the vertical velocity of the coupler face on the cask-rail car, inches/sec (The coupler on the anvil car is assumed to be stationary.)

β_{CPL} = a multiplying factor representing the fraction of F_{CPL} actually applied to the moving coupler faces

μ_{CPL} = the coefficient of friction for the sliding of the two coupler faces against each other

$\text{sgn}(\dot{Y}_{CPL})$ = signum function or sign function of $\dot{Y}_{CPL}$

The force applied to the coupler, F_{CPL}, is the coupler force, i.e.,

$$F_{CPL} = k_{SCARS}\left(X_{RC} - X_F\right) \tag{8}$$

where

k_{SCARS} = the spring constant of an equivalent single spring representing the draft gears on the cask-rail car and first anvil car, lb (force)/inch

X_{RC} = the horizontal displacement of the cask-rail car, inches

X_F = the horizontal displacement of the first anvil car, inches

The equivalent spring constant, k_{SCARS}, is defined by Equation (26) of Reference 1 as a function of the equivalent spring constants representing the draft gears on each car.

By combining Equations (6) and (7), the energy dissipated as work may be expressed as

$$W_{CRF} = -\mu_{CPL}\left|F_{CPL}\right|\text{sgn}\left(\dot{Y}_{CPL}\right)\beta_{CPL}Y_{CPL} \tag{9}$$

or

$$W_{CRF} = -\mu_{CPL}\left|F_{CPL}\right|\text{sgn}\left(\dot{Y}_{RC}-1_{CPL}\dot{\theta}_{RC}\right)\beta_{CPL}\left(Y_{RC}-1_{CPL}\theta_{RC}\right) \tag{10}$$

where

Y_{RC} = the vertical displacement of the center of gravity (c.g.) of the cask-rail car, inches

θ_{RC} = the angle of rotation of the X_{RC} and Y_{RC} axes about an axis perpendicular to the X_{RC}-Y_{RC} plane through the c.g. of the rail car, radians

l_{CPL} = the horizontal distance from the vertical centerline of the cask-rail car to the coupler face, inches

Differentiating Equation (10) with respect to each of the generalized coordinates of the system yields

$$\frac{\partial W_{CRF}}{\partial Y_{RC}} = -\mu_{CPL} \left| F_{CPL} \right| \text{sgn}\left(\dot{Y}_{RC} - l_{CPL}\dot{\theta}_{RC}\right) \beta_{CPL} \tag{11}$$

and

$$\frac{\partial W_{CRF}}{\partial \theta_{RC}} = l_{CPL}\mu_{CPL} \left| F_{CPL} \right| \text{sgn}\left(\dot{Y}_{RC} - l_{CPL}\ \dot{\theta}_{RC}\right) \beta_{CPL} \tag{12}$$

These terms have been included as energy dissipation terms in those equations of motion of the system which define the vertical and angular accelerations, $\ddot{Y}_{RC}$ and $\ddot{\theta}_{RC}$, respectively. Although the coupler force, F_{CPL}, is a function of X_{RC} and X_F, similar dissipation terms were not derived from Equation (10) for these coordinates since it was felt that an energy dissipation term for vertical motion in the equations of motion defining the horizontal accelerations did not seem appropriate. However, since the existence of these dissipation terms is indicated by the use of the energy method, further study will be made to determine if these terms should be added later.

During humping operations, the cask-rail car may impact "n" loaded cars making up a train. CARDS has been modified accordingly and now consists of the cask-rail car (hammer car) and four "anvil" cars in an "anvil train" as shown in Figure 2. Although any number of anvil cars may be considered in the anvil train, only four are in the model at present to be consistent with the make-up of the train used in the humping tests conducted at the Savannah River Laboratories from June 8, 1978 to August 3, 1978. Prior to this, the anvil train was represented by a single mass M_F, and only one coupler separated it from the cask-rail car. Now, the anvil train is represented by the

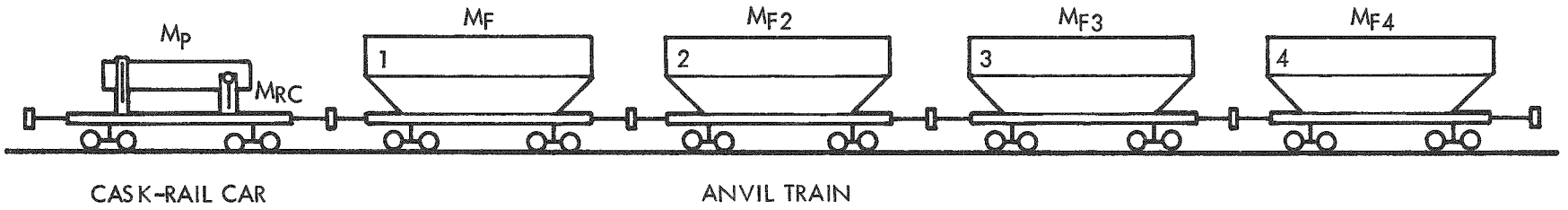

HEDL 7902-125.1

FIGURE 2. Cask-Rail Car and Anvil Train. Neg 7901733-1

four masses M_F, M_{F2}, M_{F3}, and M_{F4}, each representing a single loaded car and each separated from the other by a coupler.

The following equations of motion have been added to CARDS to accommodate the three additional anvil cars,

$$M_{F2}\ddot{X}_{F2} = k_{FF2}\ X_F - X_{F2}\ - k_{F2F3}\ X_{F2} - X_{F3}\ - \mu_{F2} W_{F2} \text{sgn}\ \dot{X}_{F2} \quad . \text{ BRKF2} \qquad (13)$$

$$M_{F3}\ddot{X}_{F3} = k_{F2F3}\ X_{F2} - X_{F3}\ - k_{F3F4}\ X_{F3} - X_{F4}\ - \mu_{F3} W_{F3} \text{sgn}\ \dot{X}_{F3} \quad . \text{ BRKF3} \qquad (14)$$

$$M_{F4}\ddot{X}_{F4} = k_{F3F4}\ X_{F3} - X_{F4}\ - \mu_{F4} W_{F4} \text{sgn}\ \dot{X}_{F4} \quad . \text{ BRKF4} \qquad (15)$$

Also, the equation of motion for the previous lumped anvil train was modified to represent the first anvil car,

$$M_F\ddot{X}_F = k_{SCARS}\ X_{RC} - X_F\ - k_{FF2}\ X_F - X_{F2}\ - \mu_F W_F \text{sgn}\ \dot{X}_F \quad . \text{ BRKIRC} \qquad (16)$$

The terms in Equations (13) through (16) are defined as follows:

M_F, M_{F2}, M_{F3}, and M_{F4} = the masses of anvil cars 1 through 4, respectively,

BRKIRC, BRKF2, BRKF3, and BRKF4 = brake switches for anvil cars 1 through 4, respectively. (Brakes are on and locked when equal to 1. and off when equal to 0.)

k_{SCARS}, k_{FF2}, k_{F2F3}, and k_{F3F4} = spring constants of equivalent springs representing the draft gear combinations between cars, lb (force)/inch

X_F, X_{F2}, X_{F3}, and X_{F4} = the horizontal displacement of anvil cars 1 through 4, respectively, inches

W_F, W_{F2}, W_{F3}, and W_{F4} = the weights of loaded anvil cars 1 through 4, respectively, lb (force)

μ_F, μ_{F2}, μ_{F3}, and μ_{F4} = coefficients of friction for sliding contact between the tracks and the wheels of anvil cars 1 through 4, respectively

The size of the anvil train may be easily varied by using switches as multipliers of the equivalent coupler springs separating the cars. Cars may be switched into or out of the train, as desired, by simply setting these switches either to 1. or to 0., respectively.

After completion of the additions and modifications discussed above, a simulation run was made to test the improved version of CARDS. Some of the input parameters for this test run are summarized in Table 1. Calculated results of the test run are presented in Figures 3, 4, and 5.

Figures 3 and 4 illustrate how the shock of impact is propagated through the train. The coupler force between cars as a function of time after impact is presented in Figure 3, and Figure 4 shows the corresponding horizontal displacements or travel of each car along the track. Rebounding and multiple collisions of the cars in the train, with energy dissipation, are illustrated in these two figures. Figure 3 shows four force peaks in rapid succession initially, due to successive bottoming of the draft gears at impact. A short time later, rebounding of the cars in reverse order occurs, that is, the last car impacted now tends to pull the rest of the train with it. This results in bottoming of the draft gears at full extension. The last car pulled, the hammer car, then rebounds in the opposite direction and again pushes the train down the track, thus completing a cycle. Friction in the draft gears and at the sliding contacts between the wheels and the track continually dissipates the energy in the system, resulting in a weakening of the force peaks after the first cycle. Some rebounding of the cars due to release of potential energy stored in the draft gears appears to occur during the first

TABLE 1

PARAMETERS USED IN SIMULATION OF RAIL CAR HUMPING TO TEST THE *CARDS* MODEL

1.	Weight of Empty Cask-Rail Car, lb_f W_{RC}	52,700
2.	Weight of Shipping Cask, lb_f W_P	140,000
3.	Weight of a Truck on Cask-Rail Car, lb_f W_{TF}, W_{TR}	7150
4.	Weight of a loaded Anvil Car, lb_f W_F, W_{F2}, W_{F3}, W_{F4}	177,000
5.	Number of Anvil Cars	4
6.	Brake Settings	
	• Cask-Rail Car	Off
	• Anvil Cars	On and locked
7.	Orientation of Cask on Car	Centered fore and aft
8.	Initial Velocity of Cask-rail Car, inches/sec VXRCI	176 (10 mph)
9.	Initial Velocity of Anvil Cars, inches/sec	0
10.	Spring Constant of "Active" Draft Gears, lb (force)/inch	48,666
11.	Spring Constant of "Solid" Draft Gears, lb (force)/inch	5×10^5
12.	Spring Constant of "Active" Suspension, lb (force)/inch	62,900
13.	Spring Constant of "Solid" Suspension, lb (force)/inch	2×10^7

TABLE 1 (Cont'd)

PARAMETERS USED IN SIMULATION OF RAIL CAR HUMPING TO TEST THE *CARDS* MODEL

14.	Coefficient of Friction for Damping in Draft Gears	0.5
15.	Coefficient of Friction for Vertical Damping at Coupler Faces	0.5
	μ_{CPL}	
16.	Coefficient of Friction for Damping in Suspension System	0.5
	μ_{D6}, μ_{D7}	
17.	Fraction of Coupler Force Used for Vertical Damping at Coupler Faces	0.1
	β_{CPL}	
18.	Fraction of Load Used for Damping in the Suspension System	0.04
	β_6, β_7	
19.	Structural Damping Coefficients, lb (force)sec/inch	10% of critical

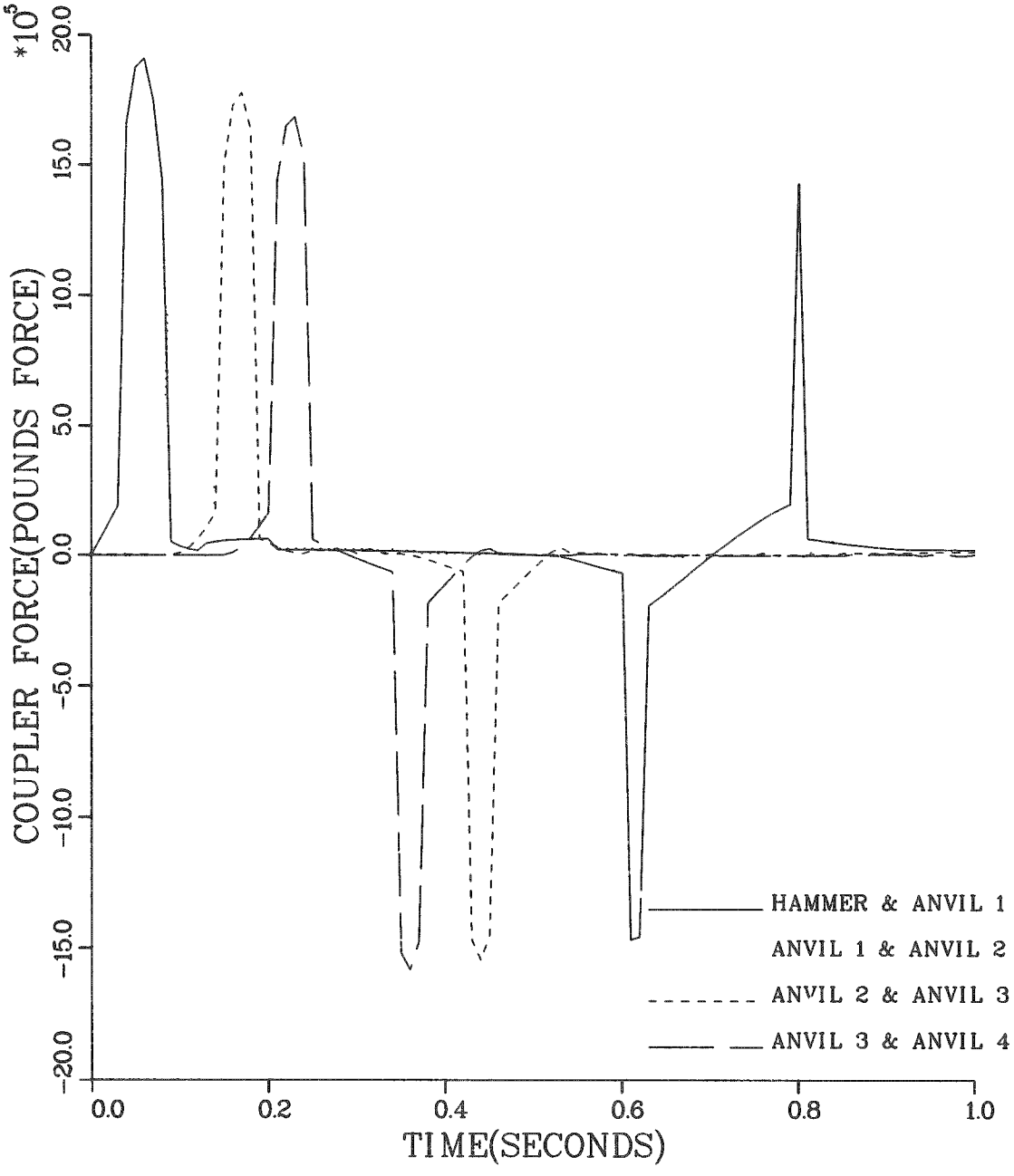

FIGURE 3. Coupler Forces Between Cars in the Cask-Rail Car and Anvil Train System.

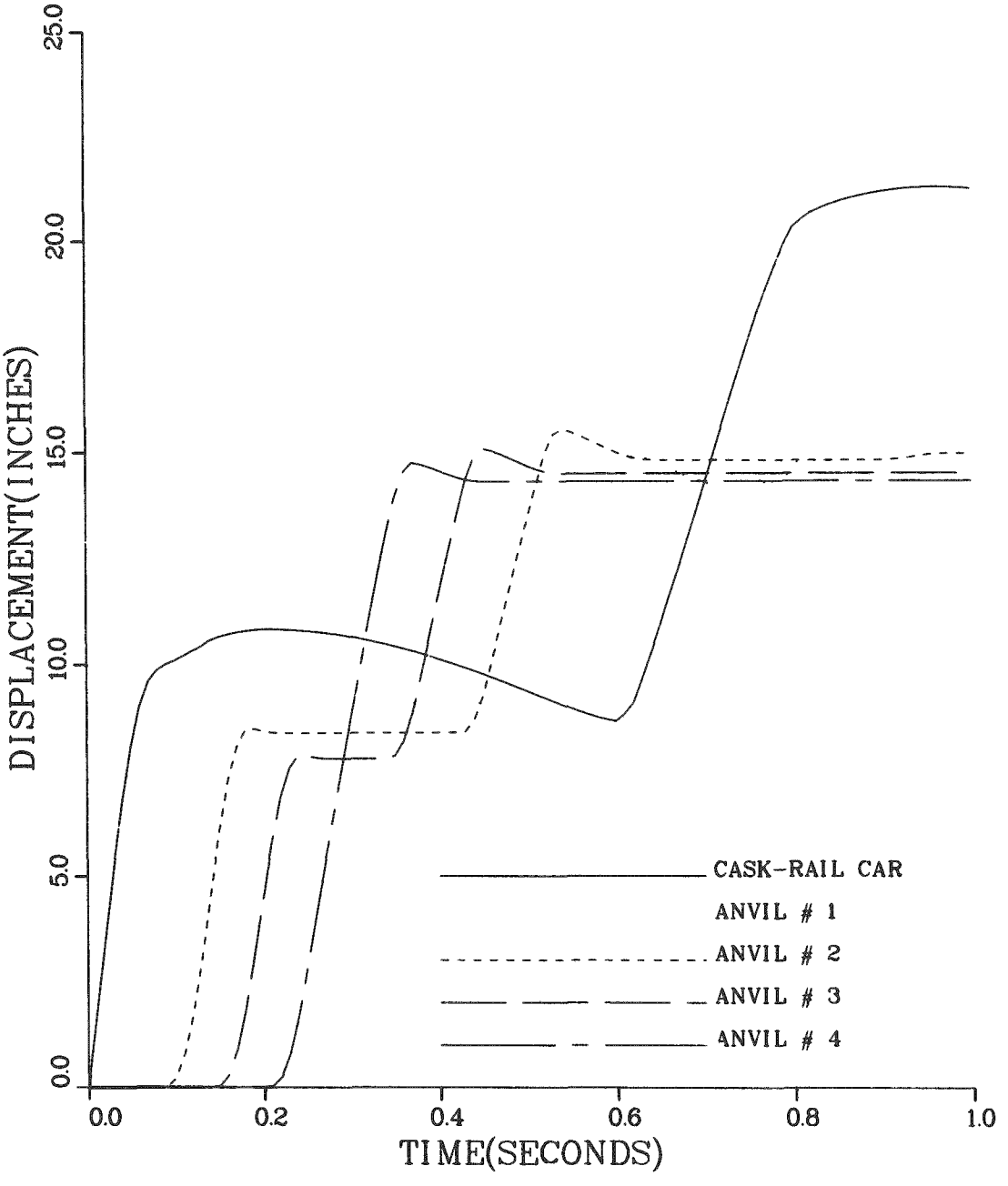

FIGURE 4. Horizontal Displacement of Cars in the Cask-Rail Car and Anvil Train System.

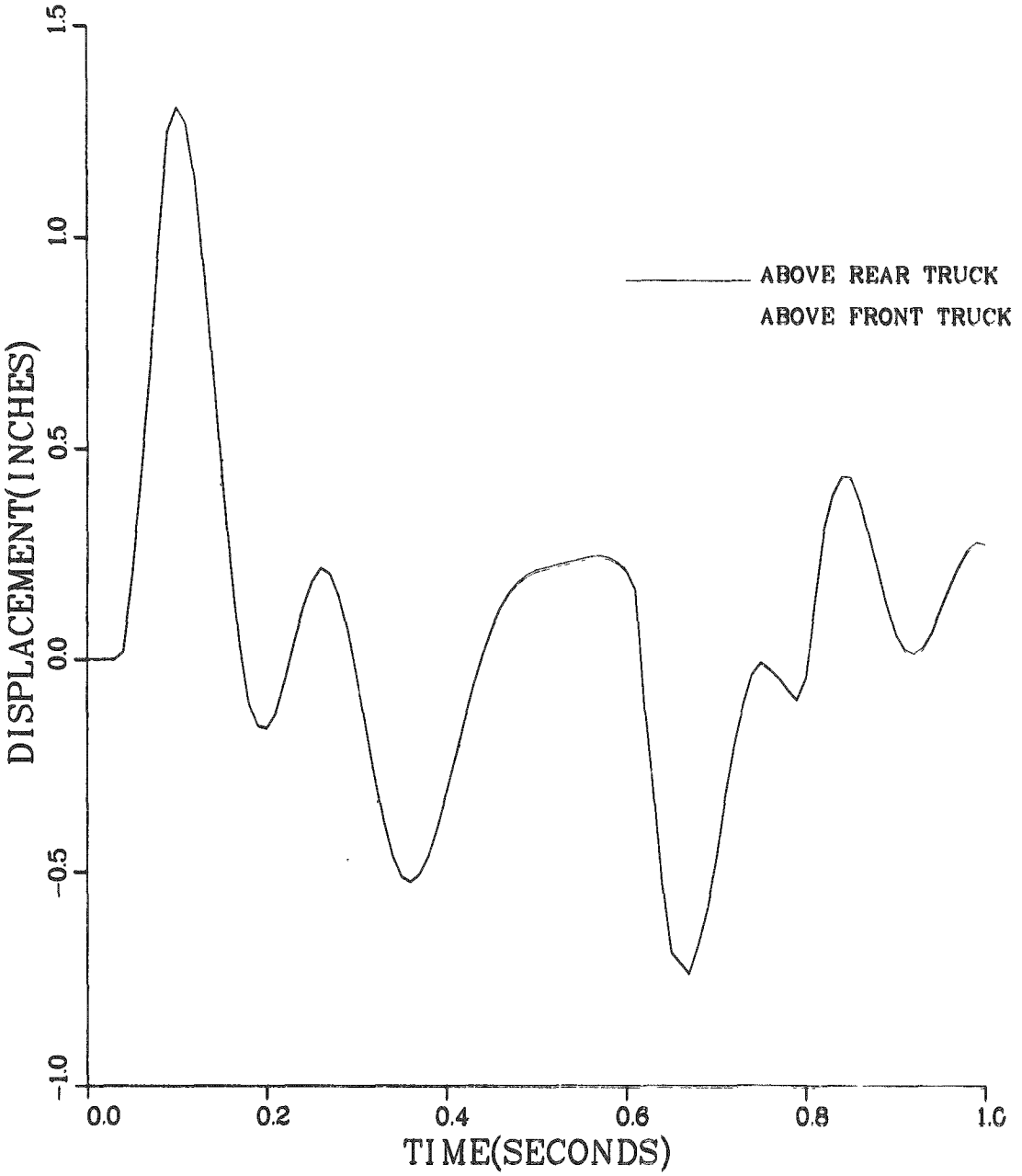

FIGURE 5. Vertical Displacement of Cask-Rail Car After Impact.

cycle, which accounts for the dips in the displacement curves in Figure 3. The dip in the displacement curve for the hammer car is more prominent than those for the other cars because it was the only car which did not have its brakes on and locked.

The vertical displacements of points on the cask-rail car, above the front and rear trucks, as a function of time after impact are shown in Figure 5. This figure illustrates both the vertical and rotational motion of the car. When the coupler bottoms out at impact, the front of the car moves downward, compressing the suspension springs, and the rear of the car moves upward. The upward displacement of the car is greater than the downward displacement for two reasons. First, the suspension system is stiffer in compression because the side force for frictional damping is proportional to the load on the system. Upward movement of the car is due to a lifting or load-relieving action with a lessening of the side force, while the downward movement is due to an intensified load with an intensification of the side force. The second reason for the greater upward displacement is the friction force at the coupler faces which opposes the direction of vertical displacement. Initially, the front of the car wants to pitch downward, but it is opposed by this frictional force and by the opposing force in the front suspension. Consequently, the less inhibited rear of the car is able to displace upward by a greater amount.

As stated earlier, the refinement of CARDS will continue throughout the study. With every improvement, and with the use of the latest parameter data, the results of each subsequent test simulation should converge toward closer agreement with "real world" situations.

A subroutine was developed for the CARDS model to convert the displacement, velocity and acceleration response of a cask-rail car system from the time domain to the frequency domain. This subroutine, developed as part of the data collection and reduction task, will allow the response spectra to be determined directly from either model output or from test data.

B. DATA COLLECTION AND REDUCTION (TASK 2)

As previously reported,[3] data recorded during the experimental tests at Savannah River Laboratories is undergoing data reduction and analysis. This report will cover representative data derived from Test 1, an 8.3 mph impact of a 70-ton SCL (Seaboard Coastline) railcar with a standard coupler, a 40-ton shipping cask, and tiedown configuration "A".[1] Tiedown configuration "A" is defined in Reference (1) as a tiedown system consisting of bolts with stops. This configuration and the location of the instruments are shown in Figure 6.

Initial analysis consisted of digitizing the analog signals at 5.12 kHz* which, according to the Nyquist sampling theorem,[4] will accurately define and preserve frequencies up to 2.56 kHz. This is consistent with the 2.5 kHz band width of information obtainable from the employed wide band FM analog recordings made at 7-1/2 IPS (IRIG intermediate band). Further, the maximum frequency of information was estimated by specialists at the Sandia Laboratories to be no greater than 1100 Hz (with instrument 7 the single exception at 2.56 kHz).

For this initial effort, every second data point from the digitized time-domain record was employed for analysis and presentation. This data selection process results in an effective sampling rate of 2.56 kHz, which preserves information content up to 1.28 kHz.

The data reduction effort during this reporting period has produced the following results which are now discussed:

- Raw time-domain data and their peak excursion values
- Filtered time-domain data and their peak excursion values
- Instant Fast Fourier Transform (FFT) for both unfiltered and filtered data
- Relative spectral energy content of filtered and raw data
- Example transfer functions

*kilo-Hz

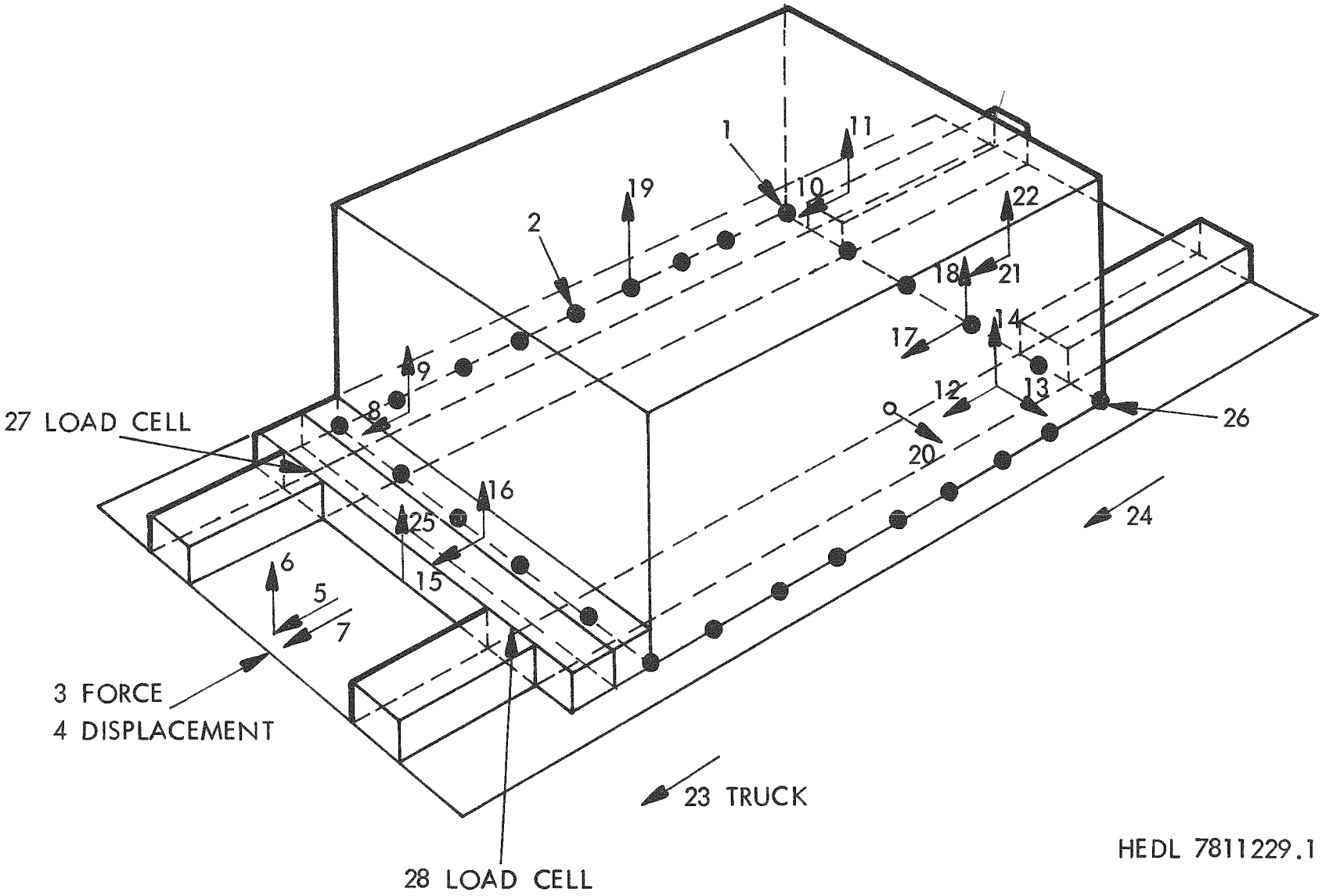

FIGURE 6. Tiedown Configuration and Instrument Location for Cask-Rail Car-Tiedown Tests (Tiedown Configuration "A"). Neg 7903318-1

Table 2 summarizes the measured and reduced parameter values from the time-domain information.

Raw time-domain data, illustrated in Figures 7 through 12, are the first 400 ms* (1024 samples of 0.39 ms/sample) following initial displacement as measured on instrument No. 4, Figure 13. These data were transformed into their frequency domain equivalent using Fast Fourier Transforms (FFT).[3] The resulting spectra, Figures 14 through 19, are measures of frequency content of the corresponding time-domain waveforms.

The representation of spectra content covers a range form DC (0th harmonic) to 1.28 kHz (512th harmonic), where a harmonic division is 2.5 Hz. The units of measure of these instant FFTs are g's/$\sqrt{Hz}$ for acceleration or k-lb/$\sqrt{Hz}$.** As in an electronic spectrum analyzer, the total harmonic content over a finite band width (2.5 Hz) must be reported at a single point, therefore a normalizing factor K is applied. To permit the magnitudes presented here to be compared with those derived by other methods of analysis, a test was developed around Parseval's formula:[5]

where $$\int_{-\infty}^{\infty} \left| f^2(t) \right| dt = K \int_{-\infty}^{\infty} \left| F^2(\omega) \right| d\omega$$

f(t) is the time-domain information

F(ω) is the Fourier Transform of f(t)

K is the applied scale factor previously mentioned

A unity magnitude sine wave was synthesized such that the sample window was equal to an integral number of periods. The resulting integral of the squared instant FFT, when compared to the integral of the original input wave square, revealed that:

---

*milliseconds

**kilo-pounds/$\sqrt{Hz}$

TABLE 2

MEASURED AND REDUCED PARAMETER VALUES FROM RAIL CAR HUMPING TESTS
(Test No. 1: 40-Ton Cask, 70-Ton Seaboard Coastline Rail Car,
Impact Velocity 8.3 mph)

DATA CHANNEL ID	INST NO.	LOCATION	MEASURED PARAMETER	RAW DATA SCALE FACTOR (SF) (FULL SCALE ±2V)	FILTERED DATA (Max/Min)	UNFILTERED DATA (Max/Min)
A	4	(SE) Car	Displacement	Timing Only	---	---
B	1	(FE) Bolt Holddown	Force	43.75 K#/V	20.21/-1.4	20.13/-2.12
C	2	(SIDE) Bolt Holddown	Force	21.88 K#/V	16.58/-2.12	16.84/-2.19
D	8	(SE) Cask	L-Acc.	±150g/V	1.5/-13.4	3.3/-13.5
E	9	(SE) Cask	V-Acc.	±62.5g/V	6/-5.4	6.25/-5.9
F	10	(FE) Cask	L-Acc.	±150g/V	1.65/-10.65	3.75/-12
G	11	(FE) Cask	V-Acc.	±62.5g/V	40/-3.69	40.63/-4.063
H	12	Car/Cask Interface	L-Acc.	±150g/V	4.65/-9.9	14.55/-18.75
J	13	Car/Cask Interface	T-Acc.	±25g/V	3.5/-3.92	10.75/-11.5
K	14	Car/Cask Interface	V-Acc.	±62.5g/V	(Impulse Noise)	(Impulse Noise)
L	17	(FE) Cask Base	L-Acc.	±100g/V	2.5/-7.9	3.5/-8.4
M	22	(FE) Car Structure	V-Acc.	±375g/V	22.1/-58.5	76.88/-155.6
N	26	(FE) Bolt Holddown	Force	35 K#/V 43.75 K#/V	10.98/-.79 13.73/-.98	11.73/-8.8 14.66/-1.1

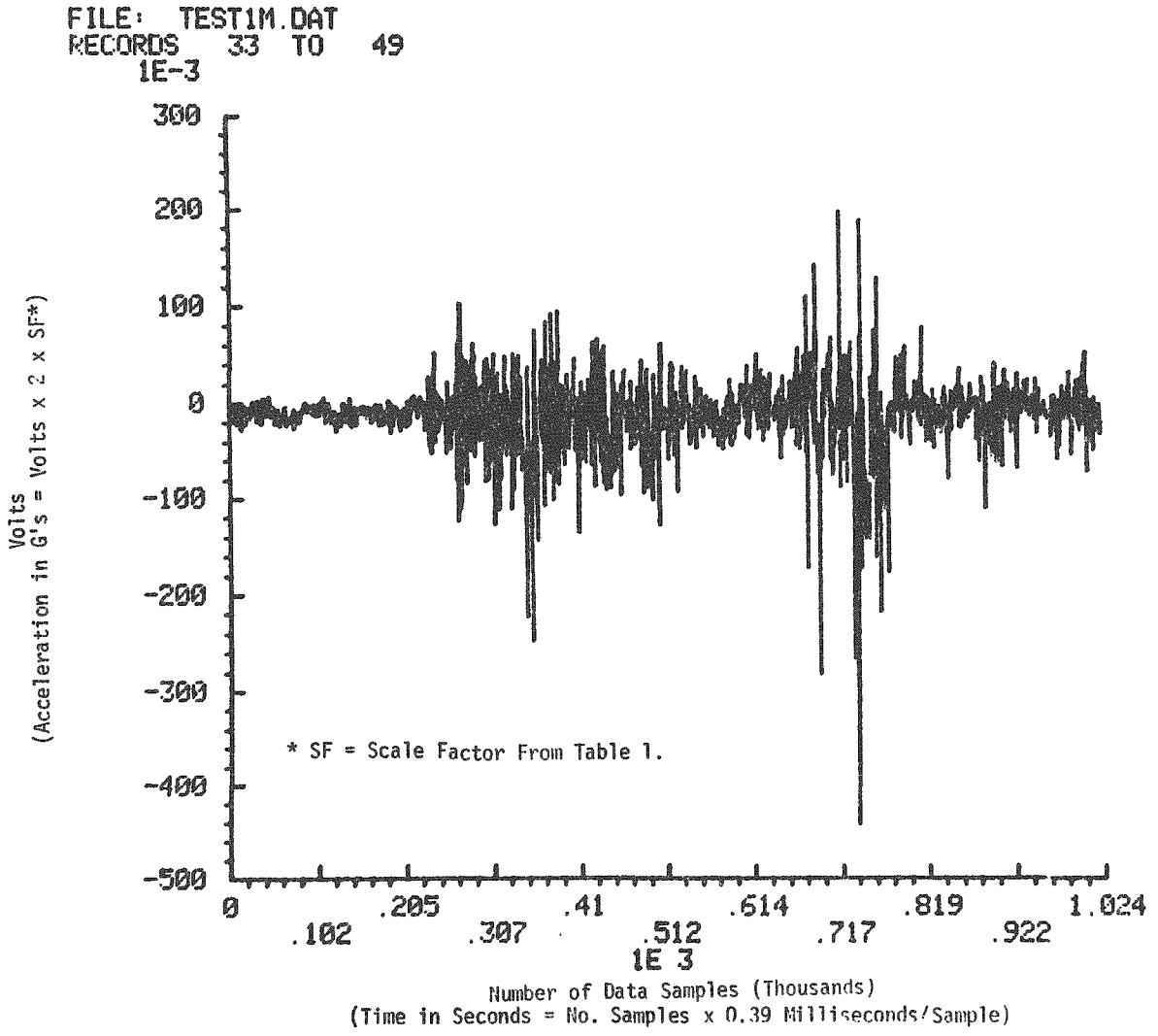

FIGURE 7. Vertical Acceleration of Car Structure at Far End vs Time (Instrument No. 22 - Unfiltered).

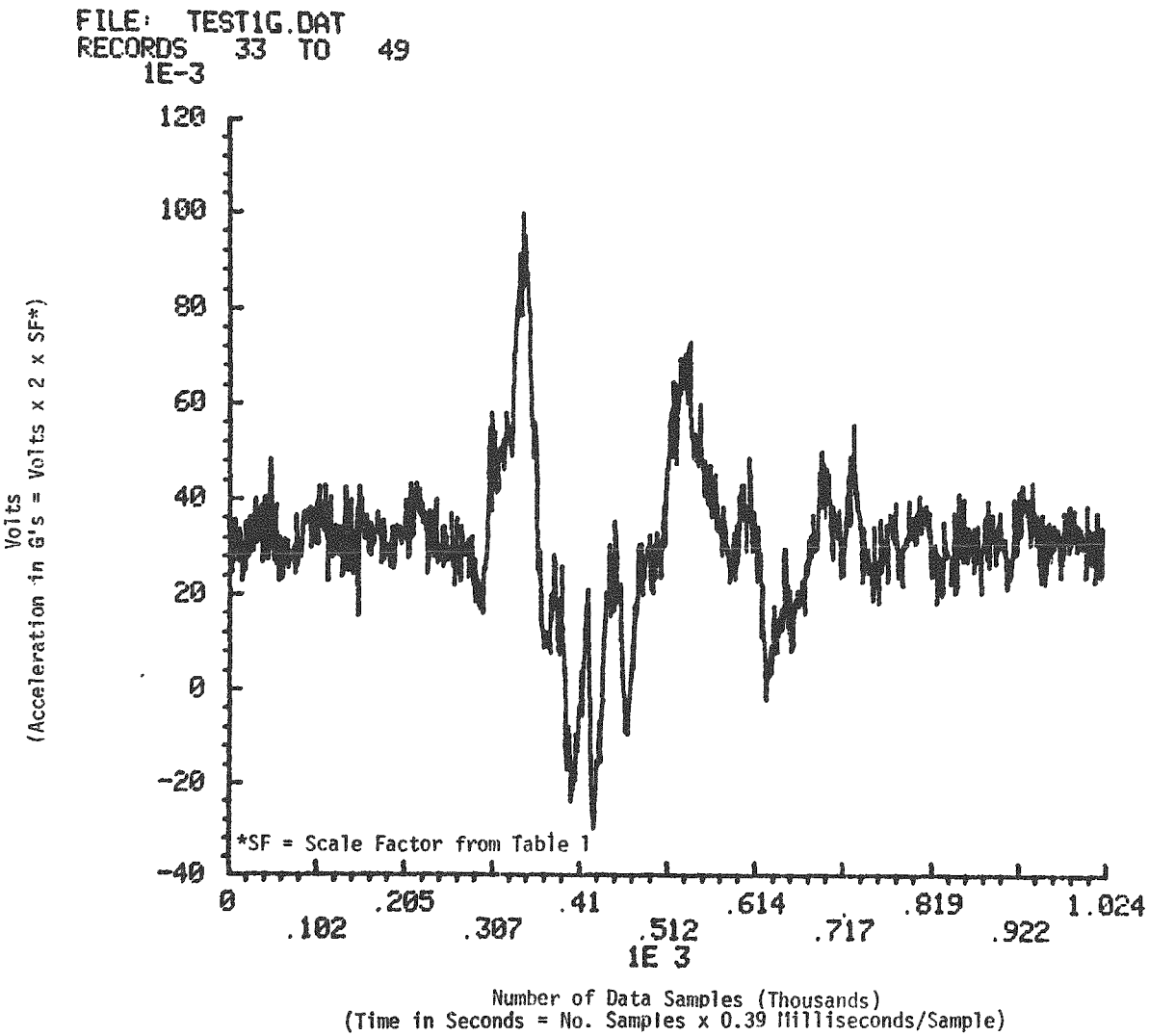

FIGURE 8. Vertical Acceleration of Cask at Far End vs Time (Instrument No. 11 - Unfiltered).

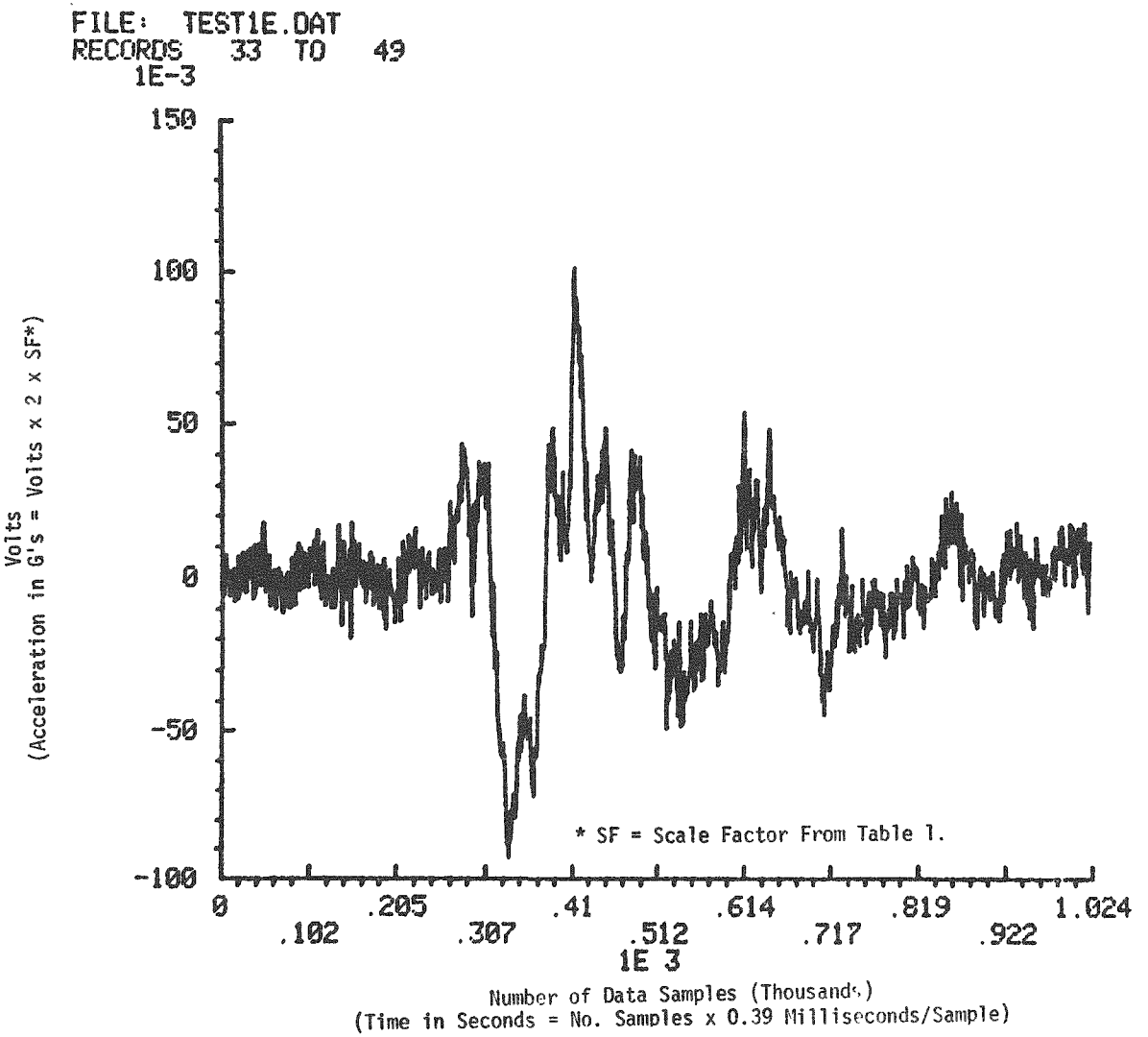

FIGURE 9. Vertical Acceleration of Cask at Struck End vs Time (Instrument No. 9 - Unfiltered).

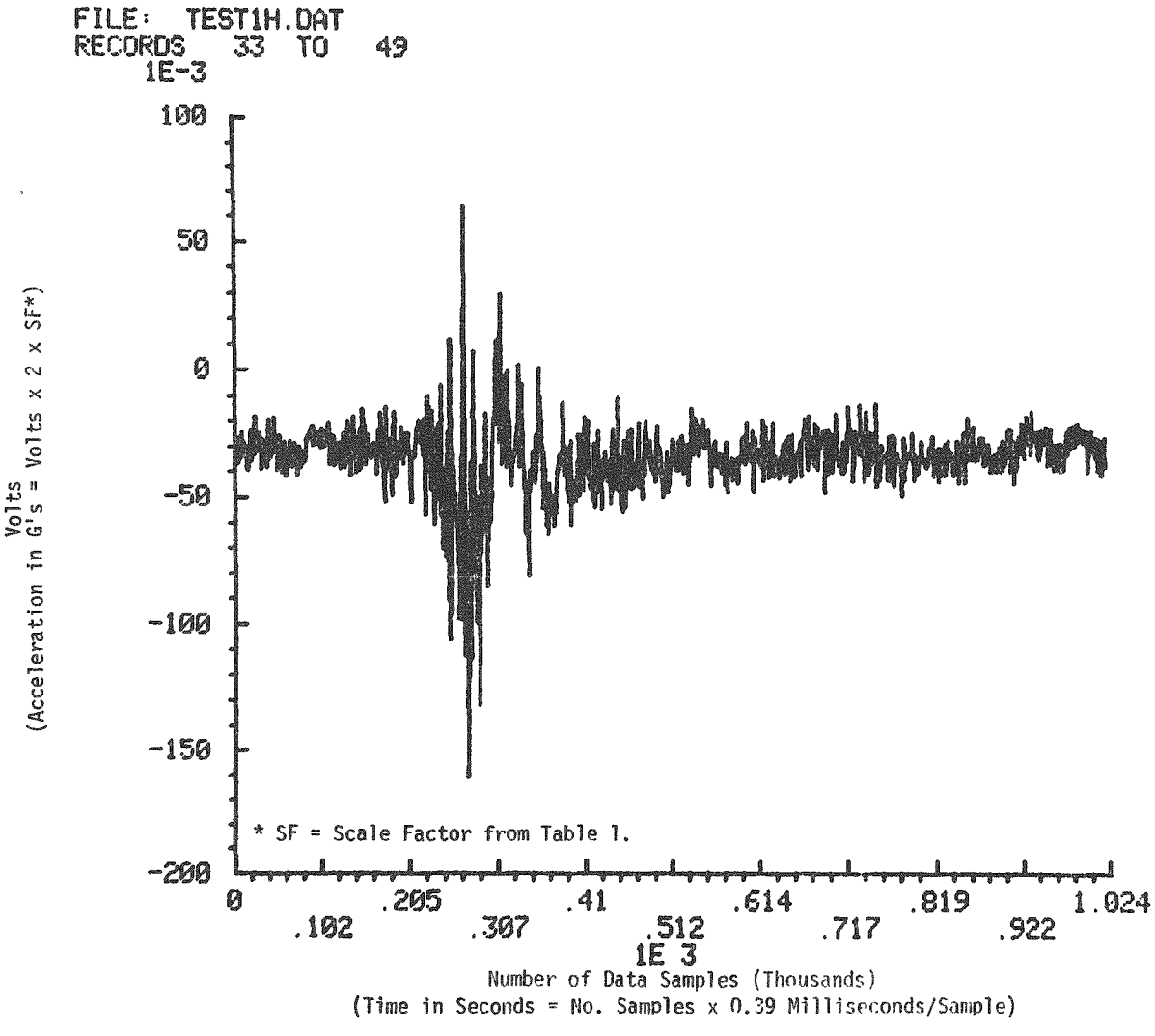

FIGURE 10. Horizontal or Longitudinal Acceleration of Car at Car/Cask Interface vs Time (Instrument No. 12 - Unfiltered).

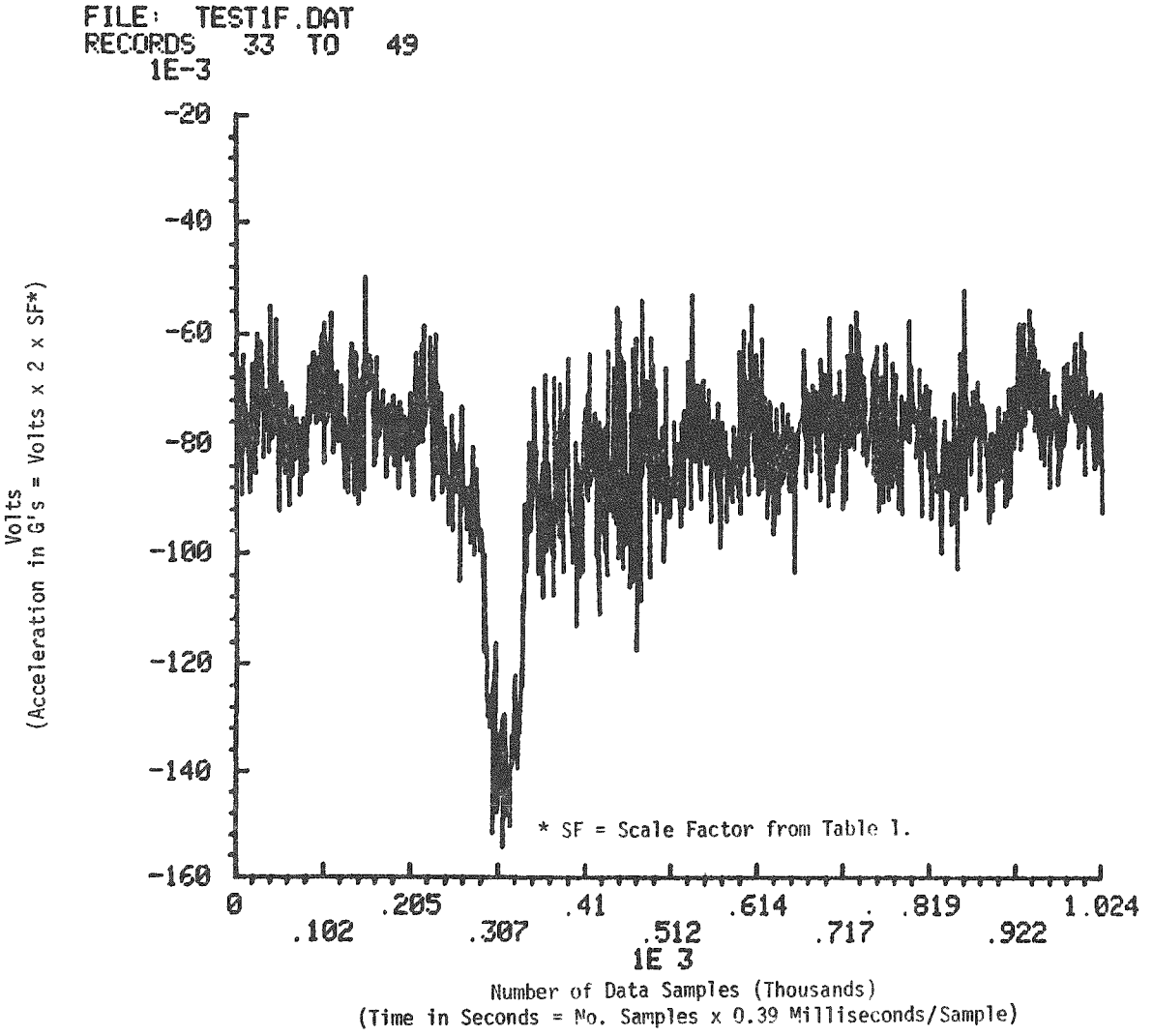

FIGURE 11. Horizontal or Longitudinal Acceleration of Cask at Far End vs Time (Instrument No. 10 - Unfiltered).

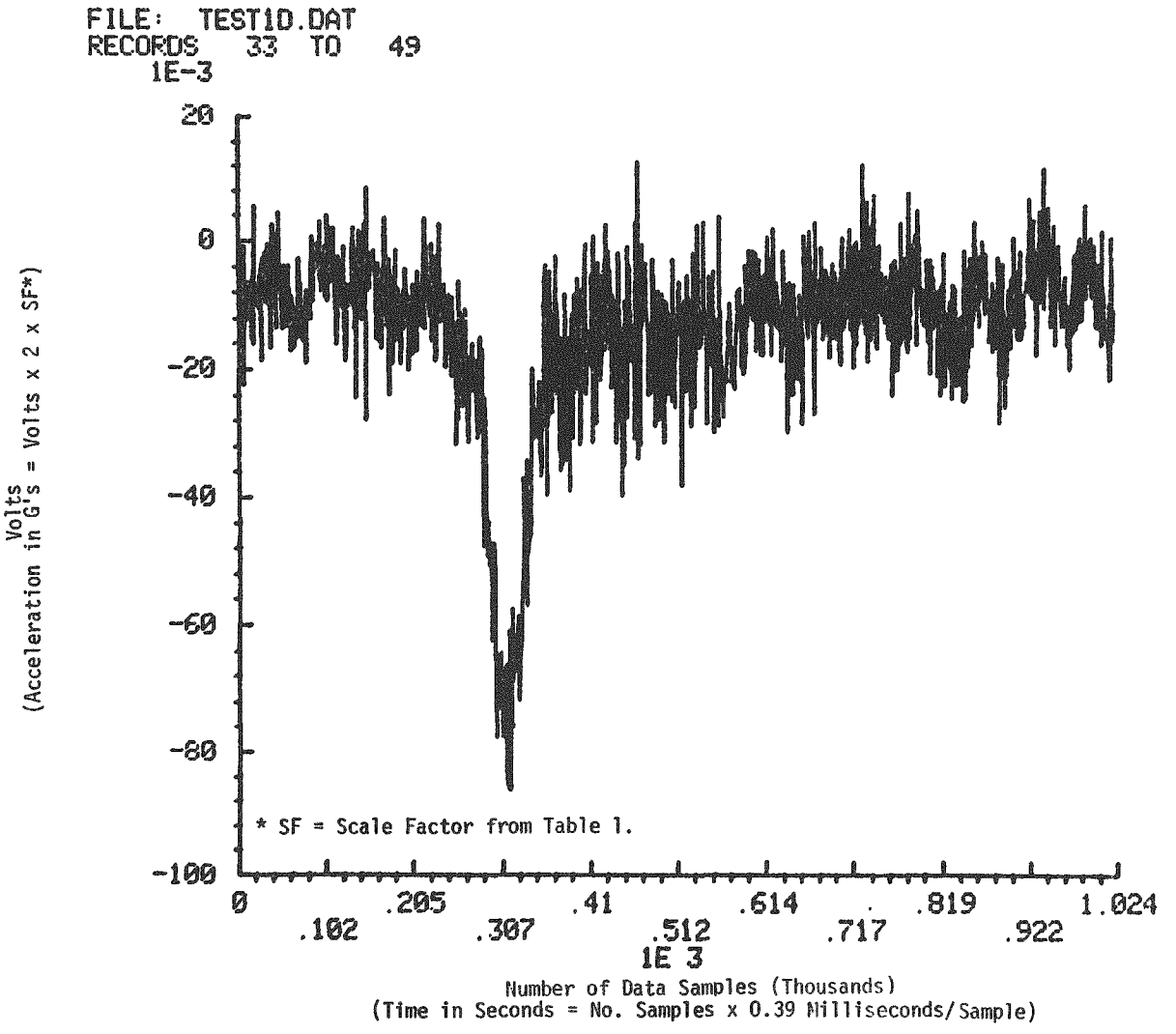

FIGURE 12. Horizontal or Longitudinal Acceleration of Cask at Struck End vs Time (Instrument No. 8 - Unfiltered).

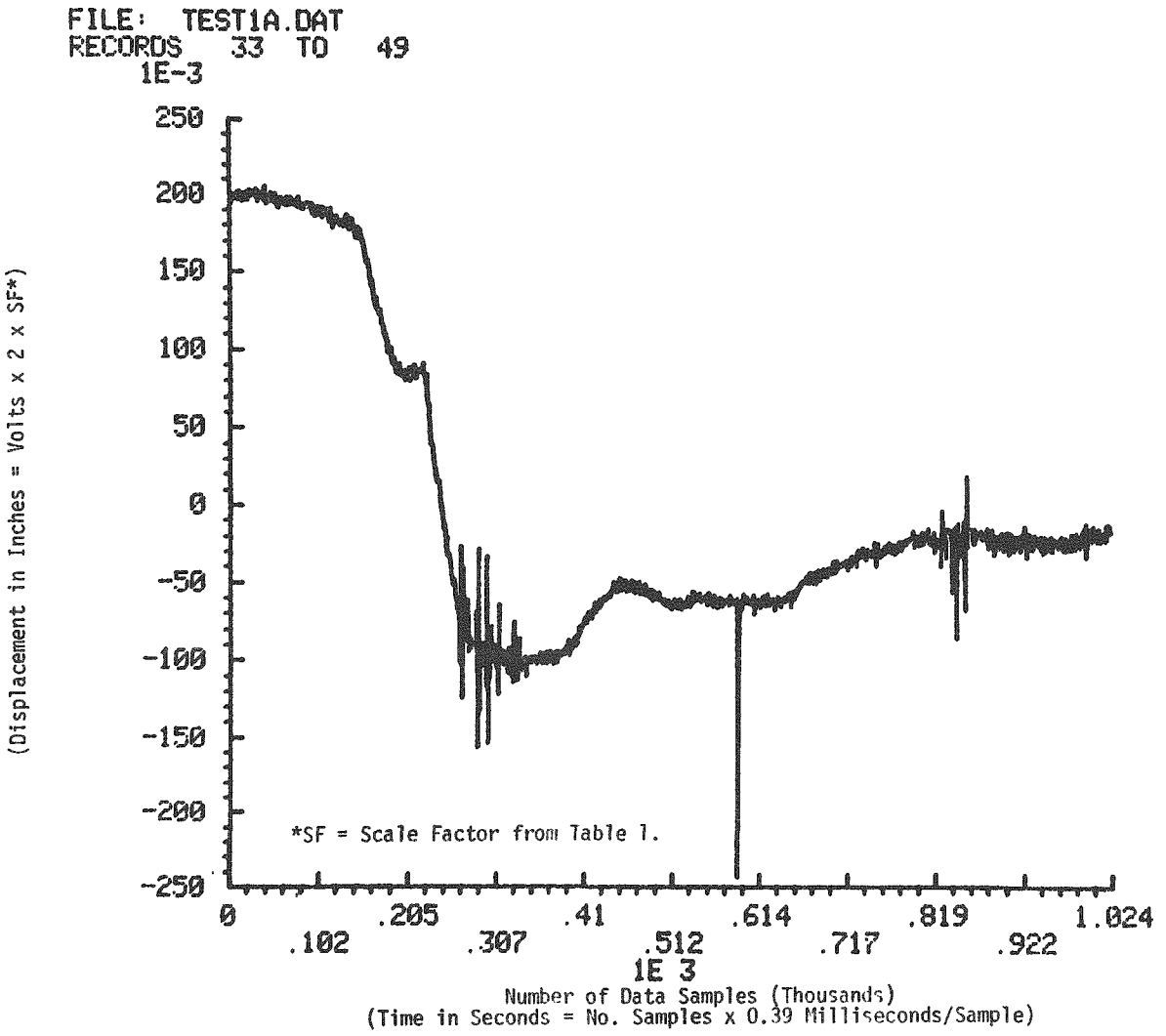

FIGURE 13. Horizontal Displacement of the Car at the Struck End vs Time (Instrument No. 4 - Unfiltered).

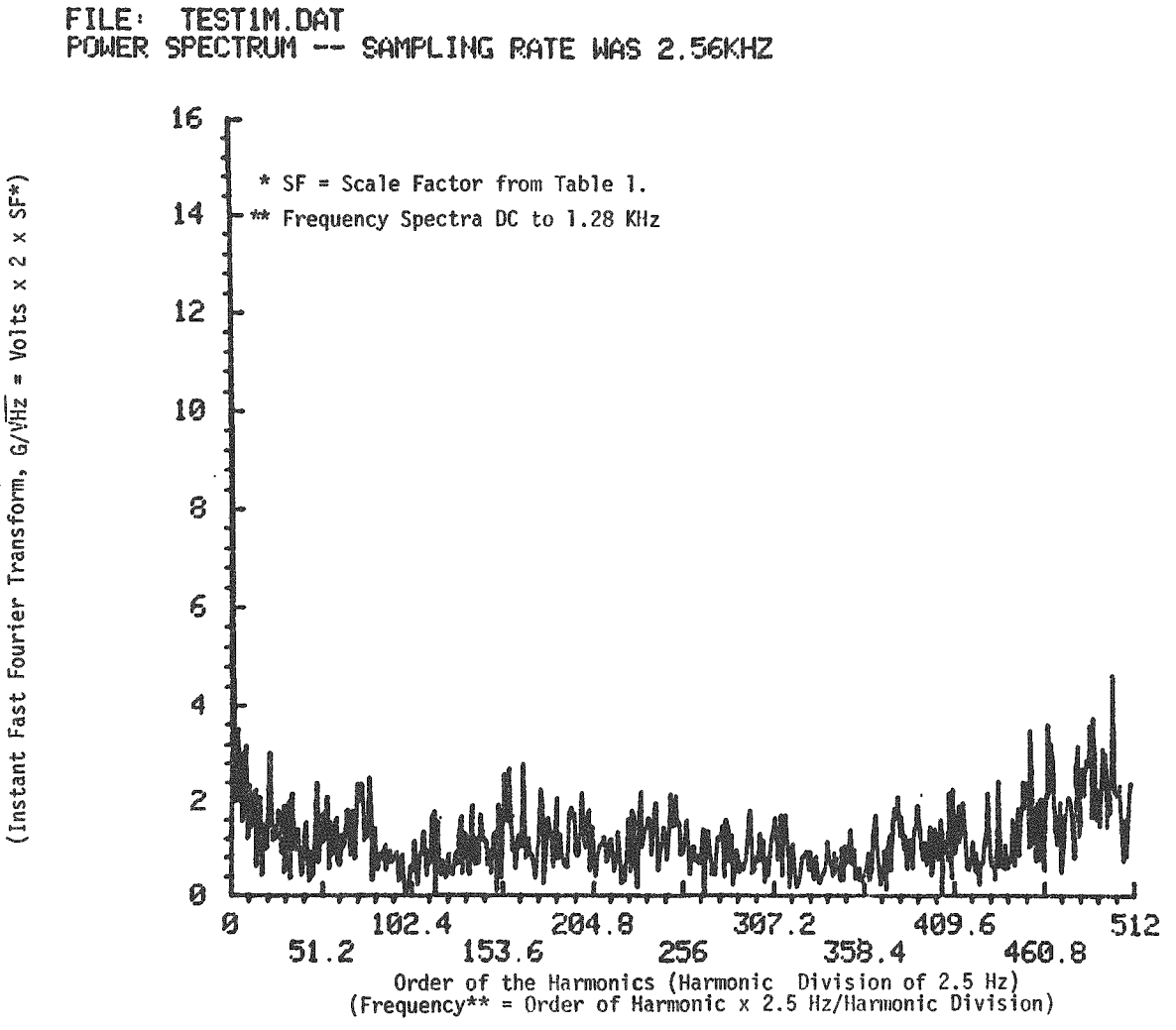

FIGURE 14. Vertical Acceleration Response of Car Structure at Far End vs Frequency (Instrument No. 22 - Unfiltered).

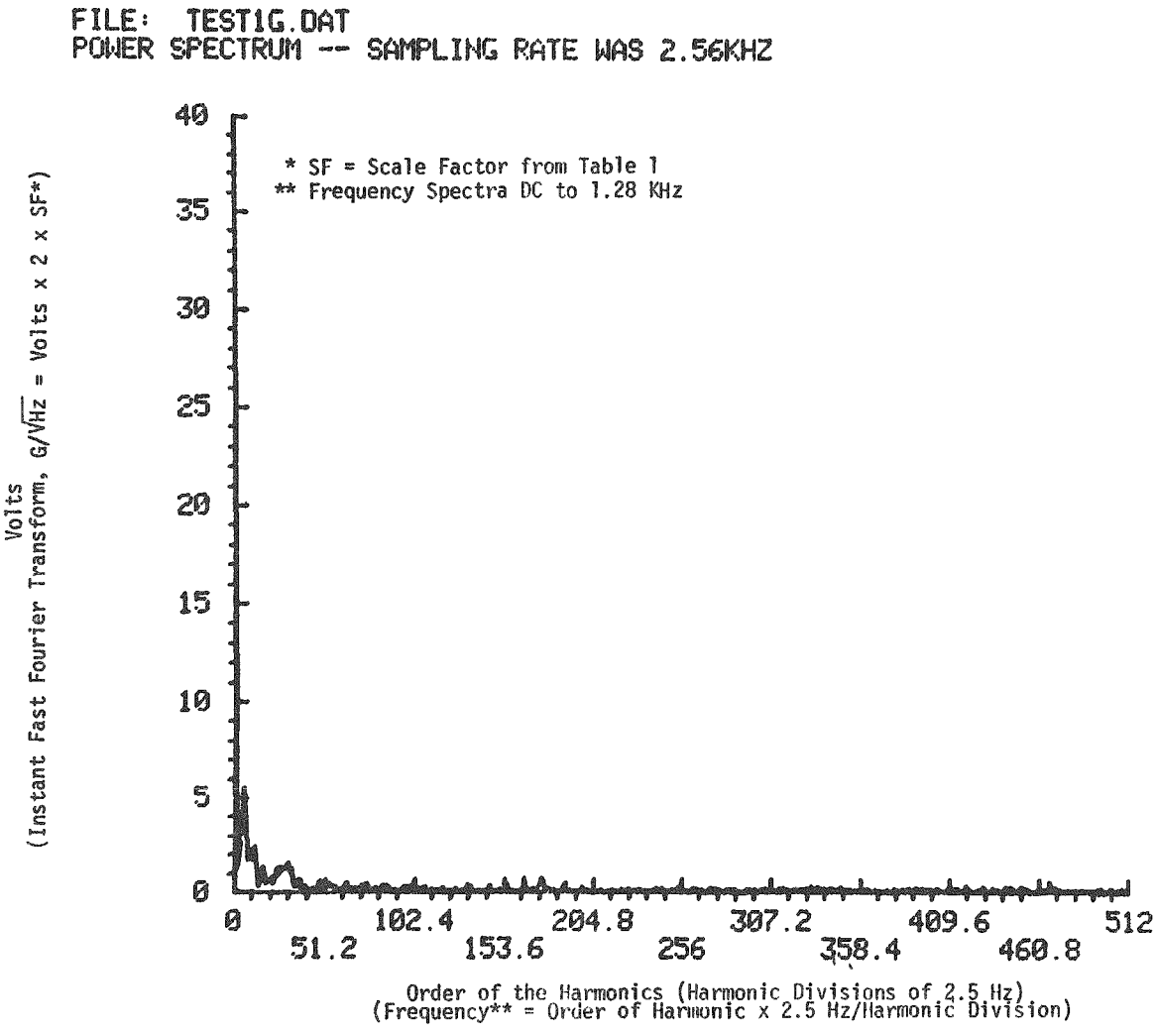

FIGURE 15. Vertical Acceleration Response of Cask at Far End vs Frequency (Instrument No. 11 - Unfiltered).

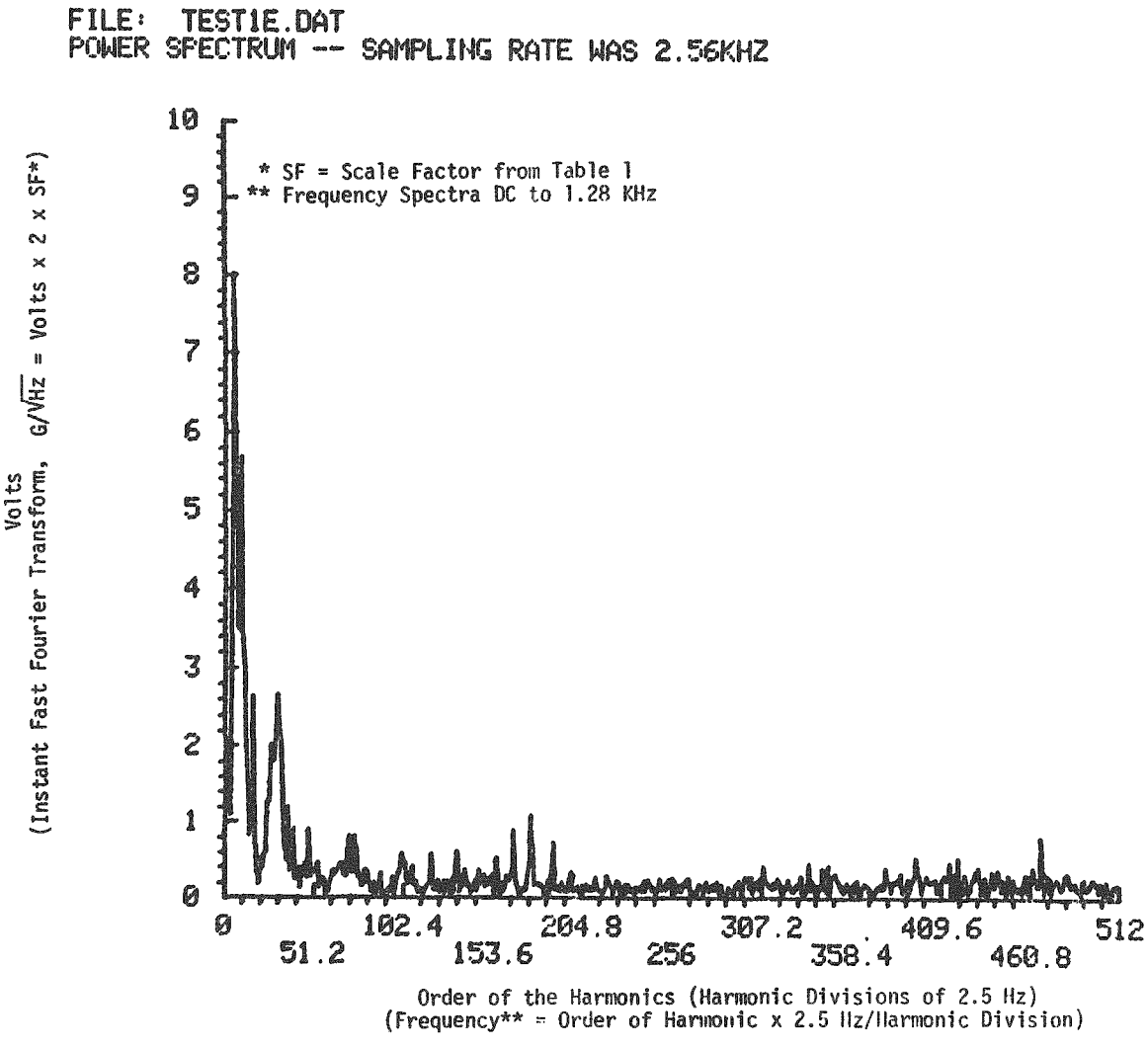

FIGURE 16. Vertical Acceleration Response of Cask at Struck End vs Frequency (Instrument No. 9 - Unfiltered).

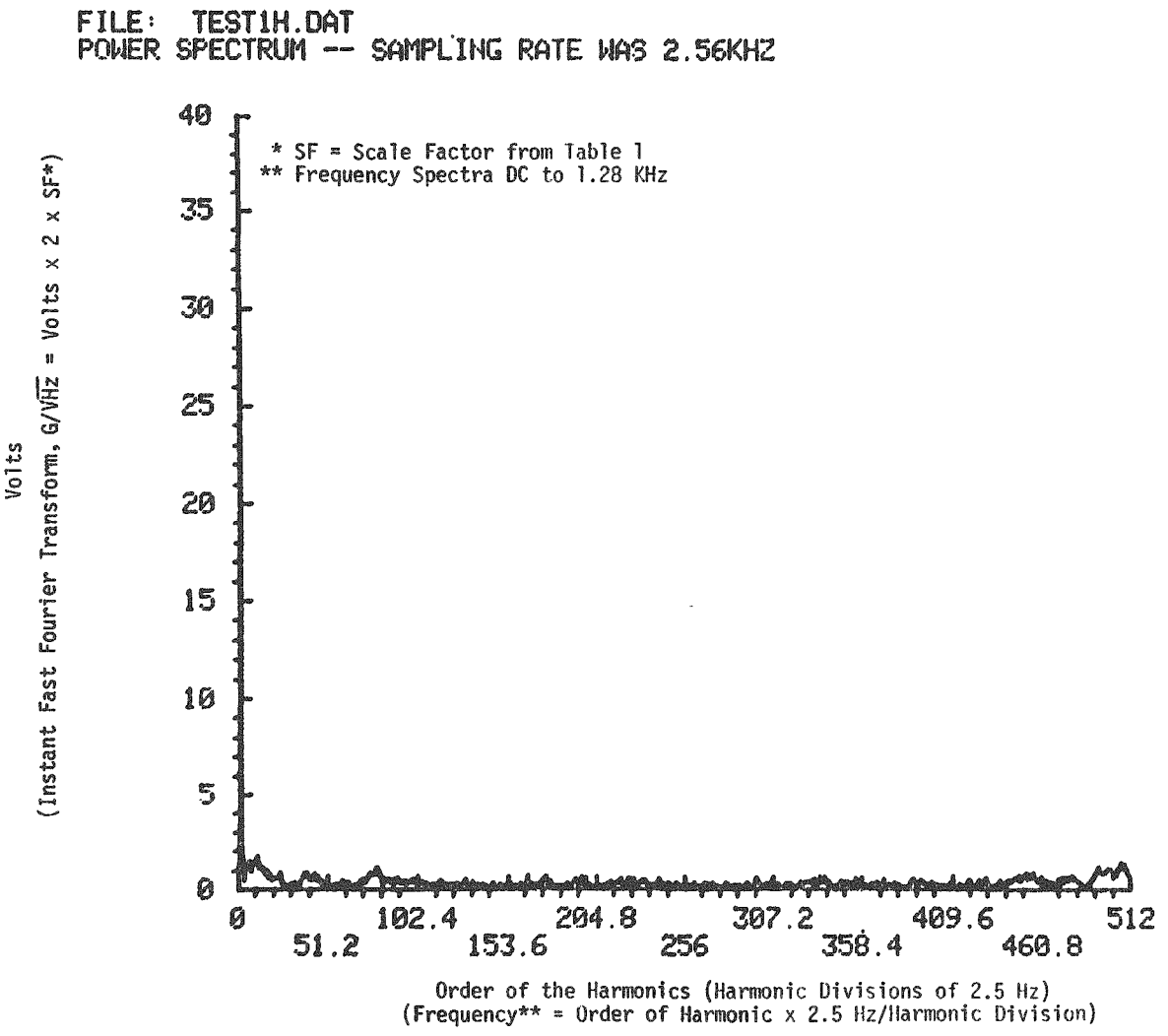

FIGURE 17. Horizontal Acceleration Response of Cask/Car Interface vs Frequency (Instrument No. 12 - Unfiltered).

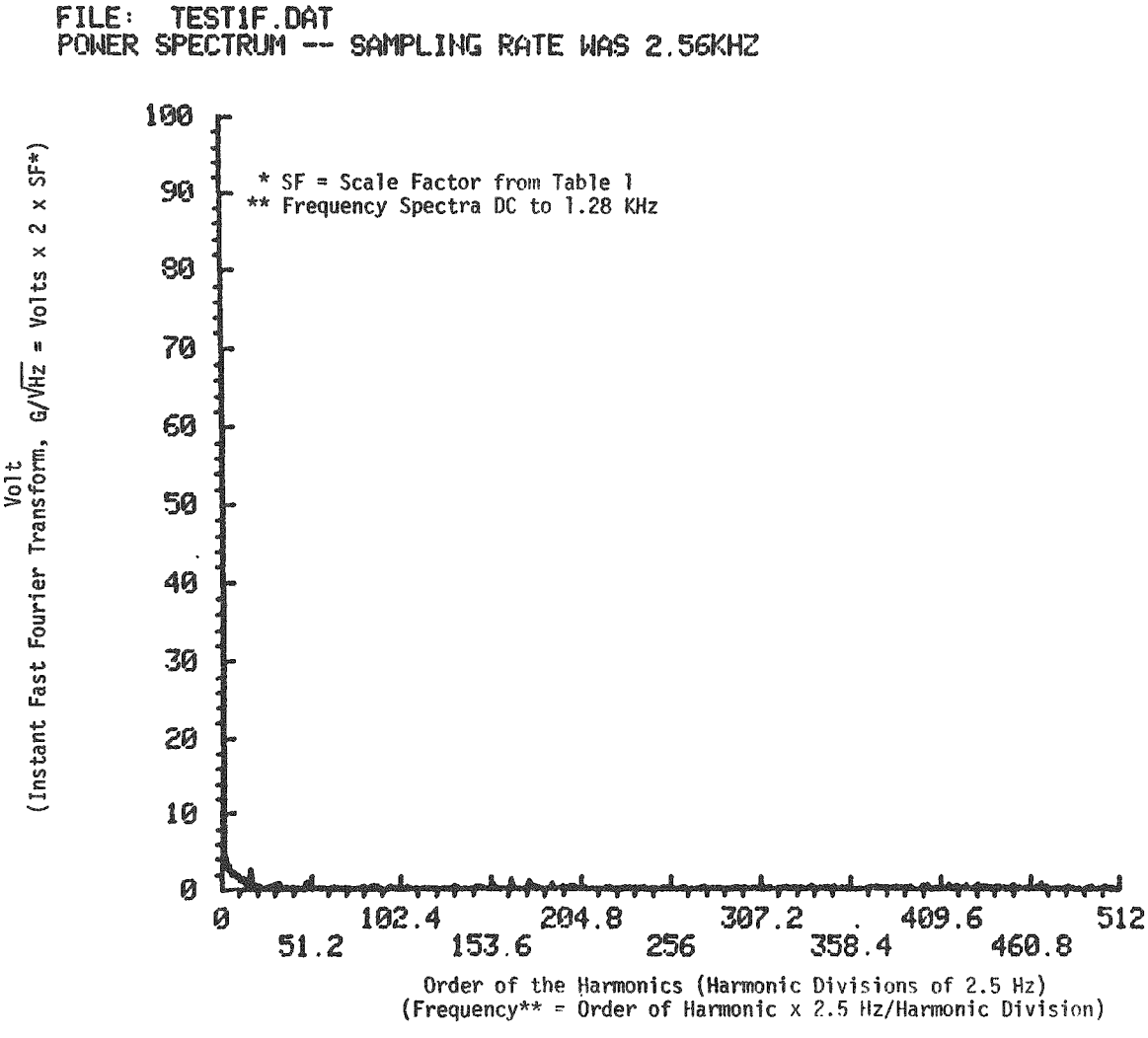

FIGURE 18. Horizontal Acceleration Response of Cask at Far End vs Frequency (Instrument No. 10 - Unfiltered).

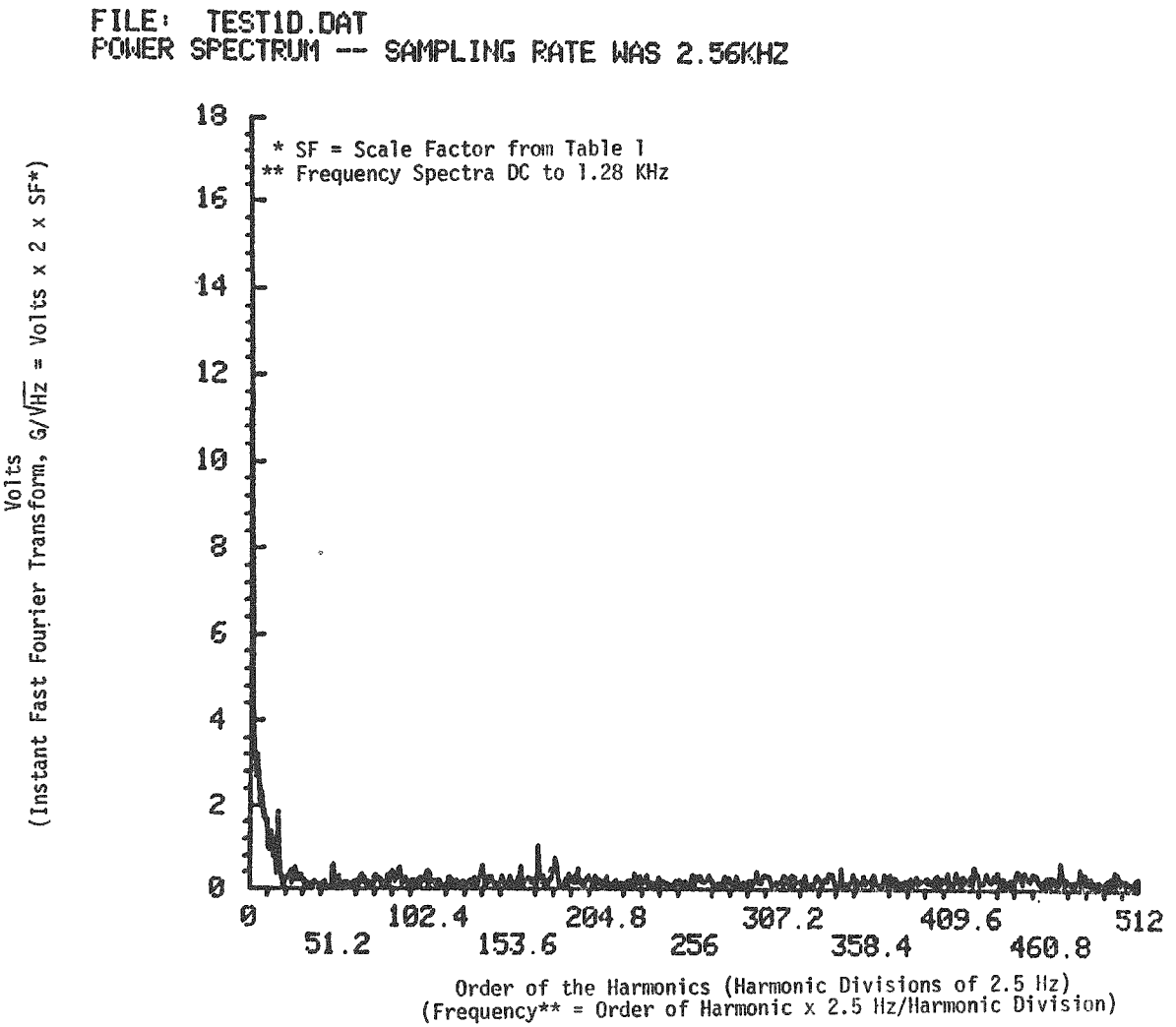

FIGURE 19. Horizontal Acceleration Response of Cask at Struck End vs Frequency (Instrument No. 8 - Unfiltered).

$$K = \frac{1}{\text{No. of Harmonics}} = \frac{2}{\text{No. of Input Samples}}$$

Since K is associated with $F^2(\omega)$ or average power spectras, the employed instant FFTs have an applied scale factor of $1/\sqrt{K}$. In the presented examples of 512 harmonics of instant FFTs, a scale factor of $\frac{1}{\sqrt{512}}$ or 0.0442 has been incorporated.

One of the objectives of this empirical data analysis is to provide information to validate the analytical model. It was determined that by analyzing a narrow band of frequencies rather than the entire spectrum, a first-order solution would be more easily obtained. Further, if the energy content of that narrow band represented the major portion of the total energy, further analysis might be minimized. Using the symmetric properties of the FFT, ideal filtering was performed by truncating the frequency at the 100th harmonic (250 Hz) and performing an inverse FFT.

Table 3 compares the energy in the band-width limited spectra to the energy of the entire spectra, for selected examples of acceleration data. These data are shown as unfiltered time-domain information in Figures 7 through 12, and as filtered time-domain data in Figures 20 through 25. It is apparent that the time-domain peak values may be significantly reduced when the eliminated high frequency energy represented an appreciable portion of the entire spectrum. Note that this energy relationship is a necessary but not sufficient condition to cause the peak value variations.

Also related to the limited band width energy distribution is the range of effectiveness of a transfer function $\overline{H}(\omega)$.[3] Transfer functions are essentially ratios of corresponding instant FFTs derived from the input and output of the system. This function represents the system's output response to an input stimuli of a single frequency. If incomplete parameters are employed to represent the system's response, the response is incompletely characterized. However, the system is accurately characterized over that limited range. The data presented here consider the band of frequencies DC

TABLE 3

SELECTED POWER SPECTRA ENERGY COMPARISONS
FOR LIMITED BAND WIDTH DATA

$$R(\omega_1, \omega_2) = \frac{\int_0^{\omega_2} \left| F^2(\omega) \right| \, d\omega}{\int_0^{\omega_1} \left| F^2(\omega) \right| \, d\omega}$$

where R = represents energy ratio

$F(\omega)$ = instant FFT

ω_1 = highest frequency analyzed 1.28 kHz

ω_2 = cut-off frequency 250 Hz

Instrument No.	R
9	.932
11	.993
22	.366
8	.931
10	.996
12	.956

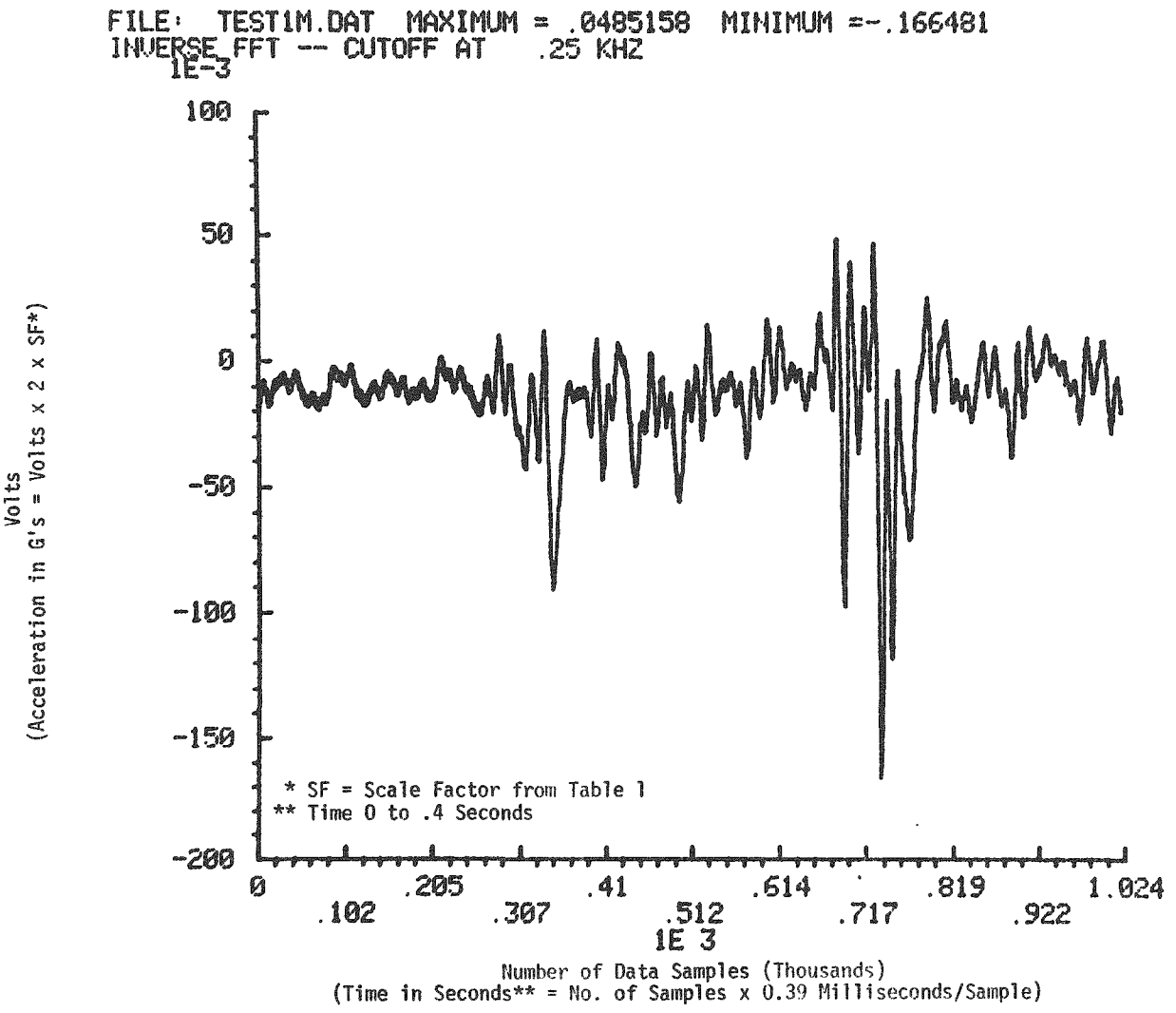

FIGURE 20. Vertical Acceleration of Car Structure at Far End vs Time (Instrument No. 22 - Filtered at 250 Hz).

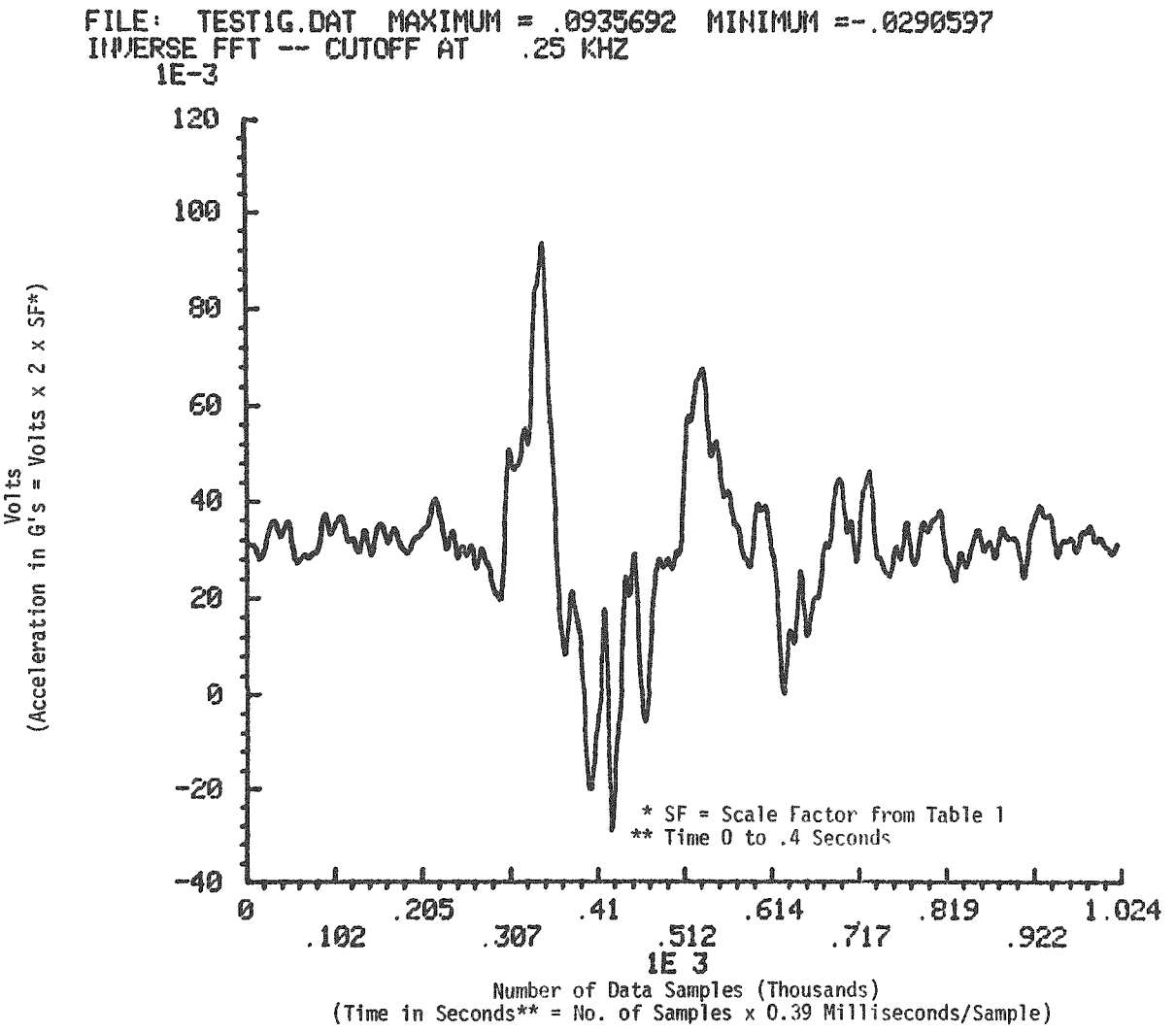

FIGURE 21. Vertical Acceleration of Cask at Far End vs Time (Instrument No. 11 - Filtered at 250 Hz).

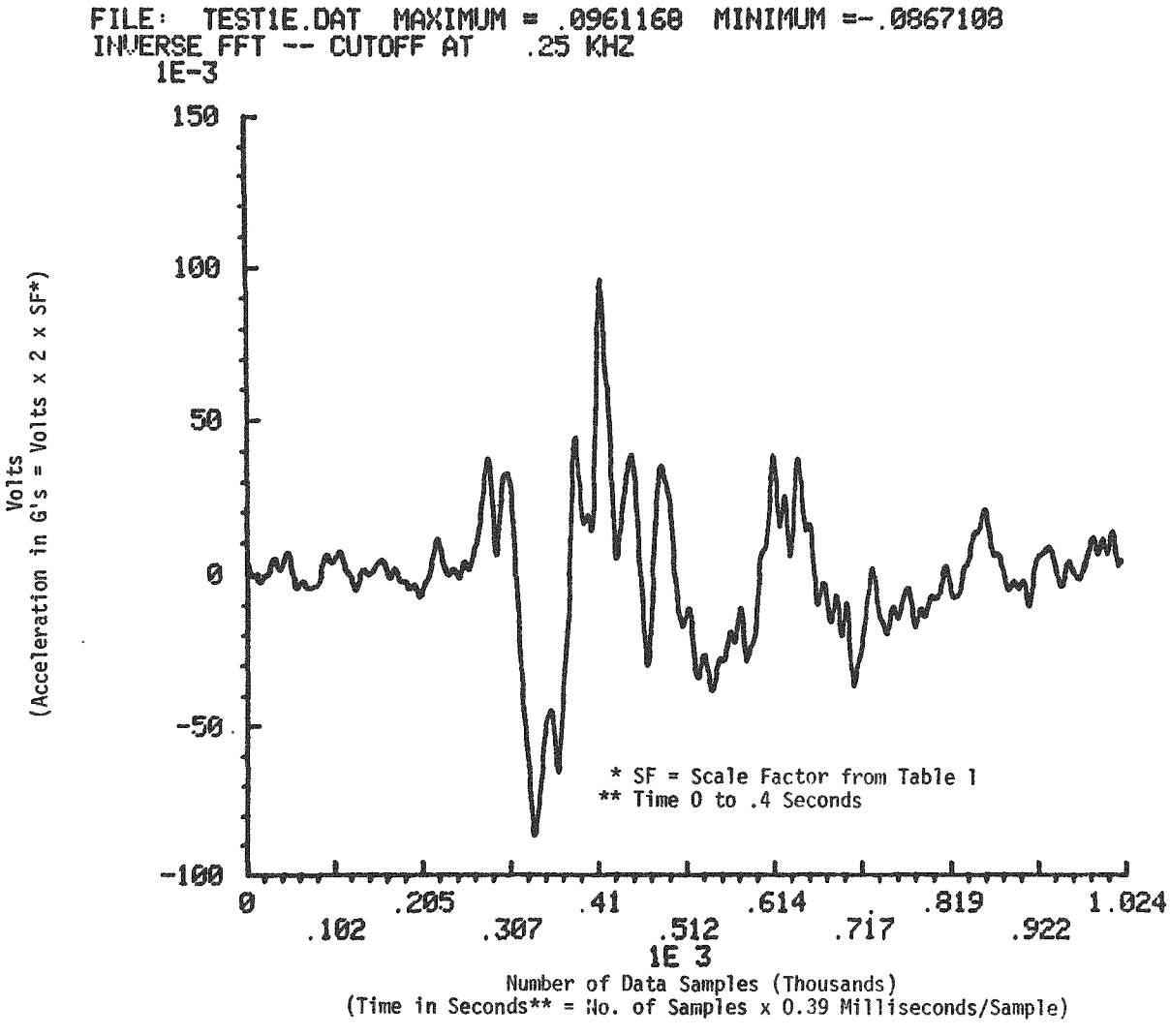

FIGURE 22. Vertical Acceleration of Cask at Struck End vs Time (Instrument No. 9 - Filtered at 250 Hz).

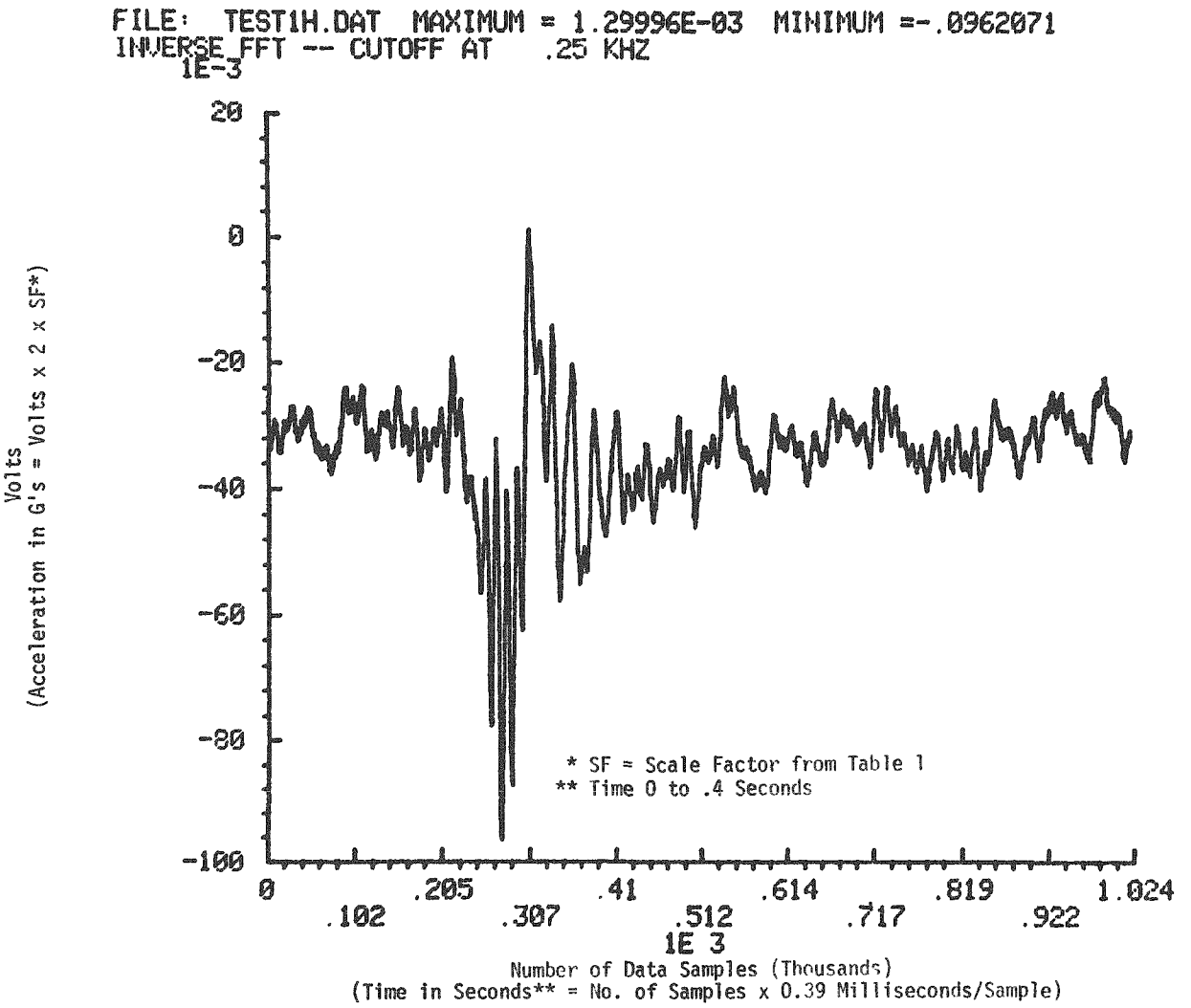

FIGURE 23. Horizontal Acceleration of Car at Car/Cask Interface vs Time (Instrument No. 12 - Filtered at 250 Hz).

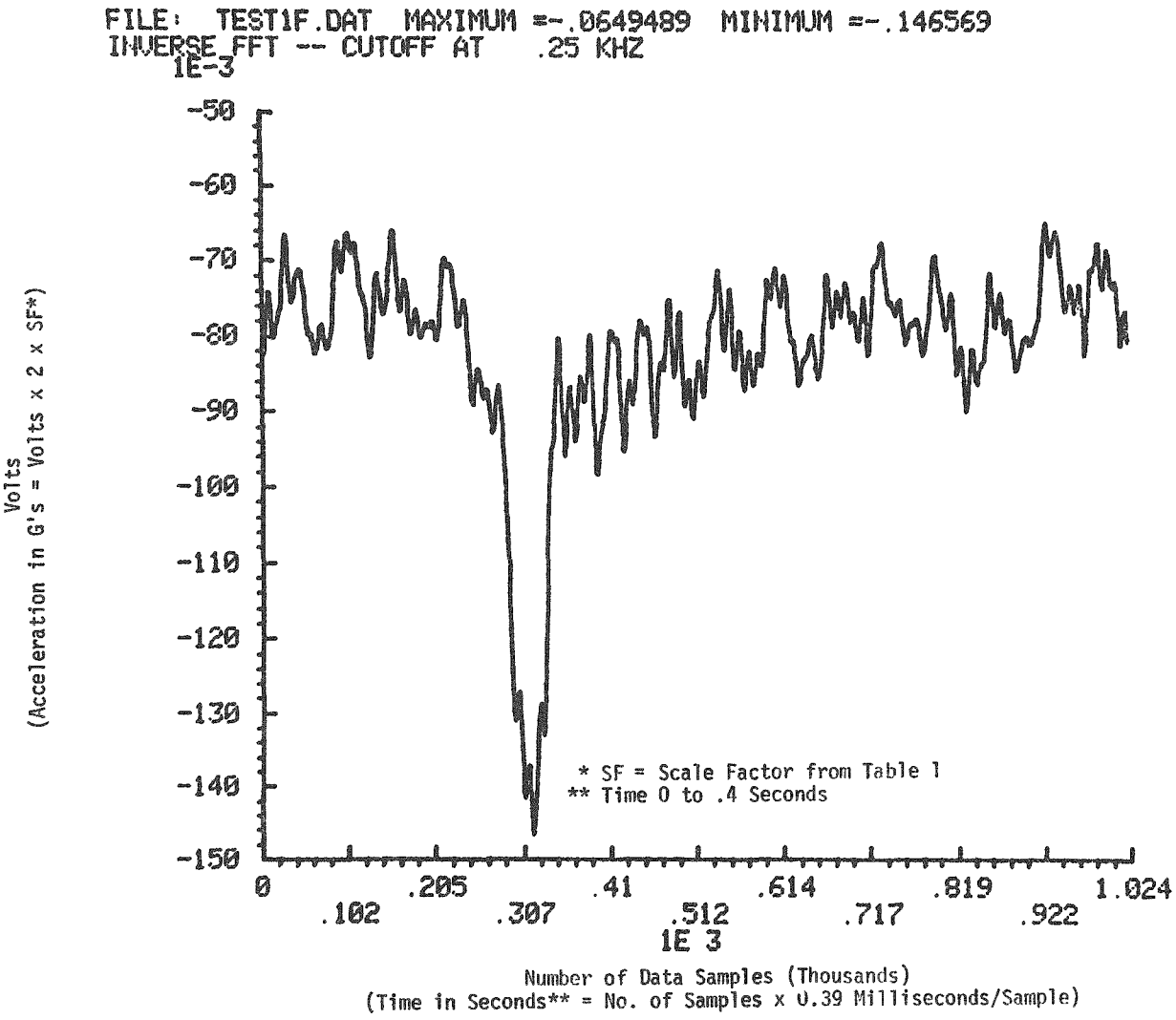

FIGURE 24. Horizontal Acceleration of Cask at Far End vs Time (Instrument No. 10 - Filtered at 250 Hz).

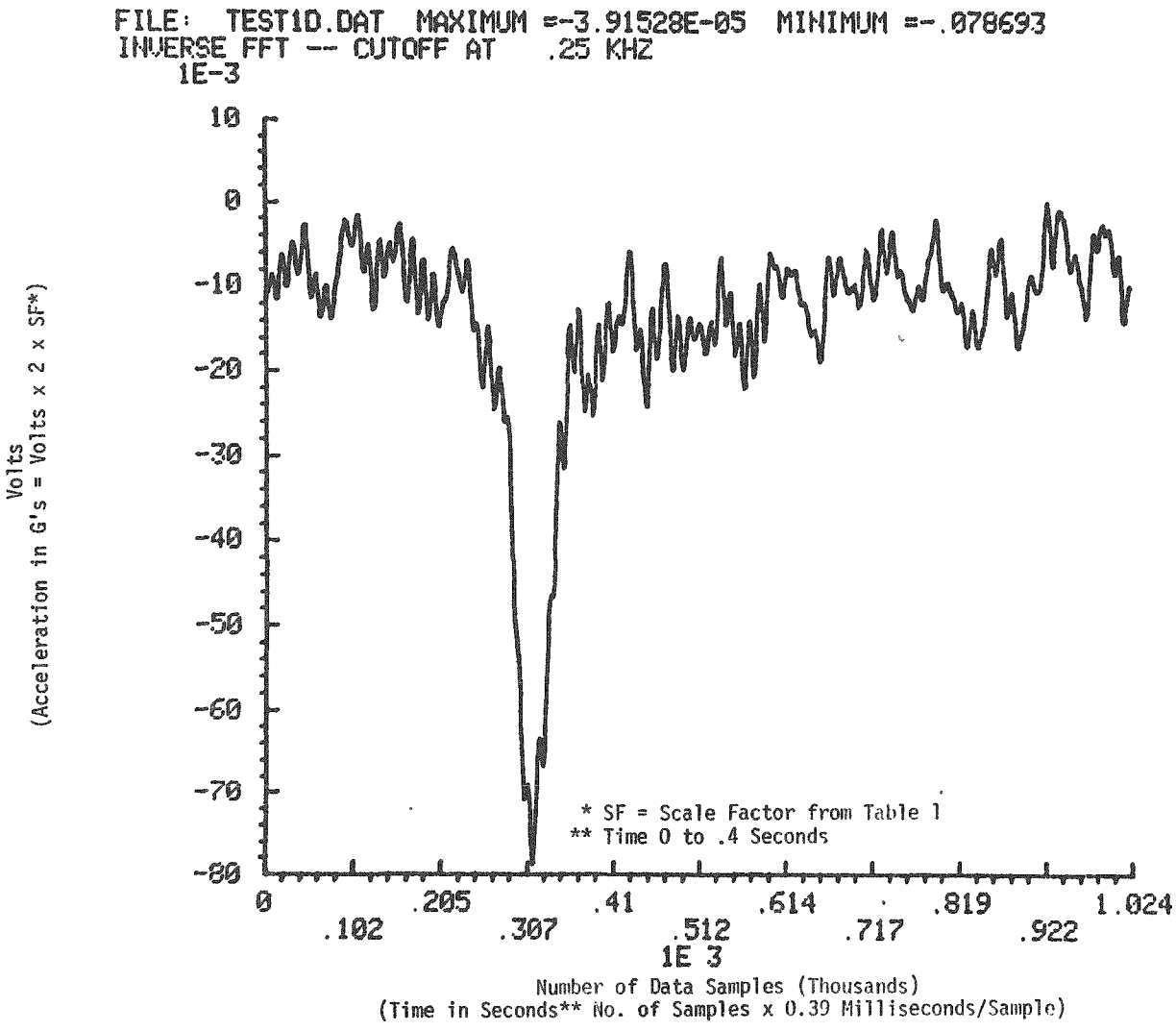

FIGURE 25. Horizontal Acceleration of Cask at Struck End vs Time (Instrument No. 8 - Filtered at 250 Hz).

to 250 Hz. The assumption is made that system noise is above 250 Hz, but no attempt has been made to characterize or to quantify that noise.

Figures 26 and 27 illustrate the transfer function magnitude relating the energy transfer from instrument 22 to 11 and from instrument 11 to 9 over the frequency range DC to 250 Hz. This corresponds to the vertical transfer of energy from the far end of the car on its structure, to the far end of the cask; then to the struck end of the cask. These figures show that $|\bar{H}| > 1$. Therefore, the energy is transferred from 9 to 11 (from the struck end to the far end) rather than the direction shown (11 to 9).

In a similar fashion, Figures 28 and 29 illustrate the longitudinal energy transfer characteristics from 12 to 10 and 10 to 8. Again observing the value of $|\bar{H}|$ relative to 1, general characteristics of energy couplings directions are revealed. In this case the direction is related to frequency in a complicated manner relative to the simple paths assumed.

The results of these efforts illustrate the techniques which are being employed for data reduction. They show the applicability of analyzing the band width limited data as a first step towards model verification. Completed data analysis results are scheduled to be reported during the next quarter.

C. VALIDATE MODEL (TASK 3)

This task has been rescheduled to a later date.

D. COLLECT PARAMETER DATA (TASK 4)

There has been no activity in this task during this reporting period.

E. PARAMETRIC AND SENSITIVITY ANALYSIS (TASK 5)

This task has been rescheduled to a later date.

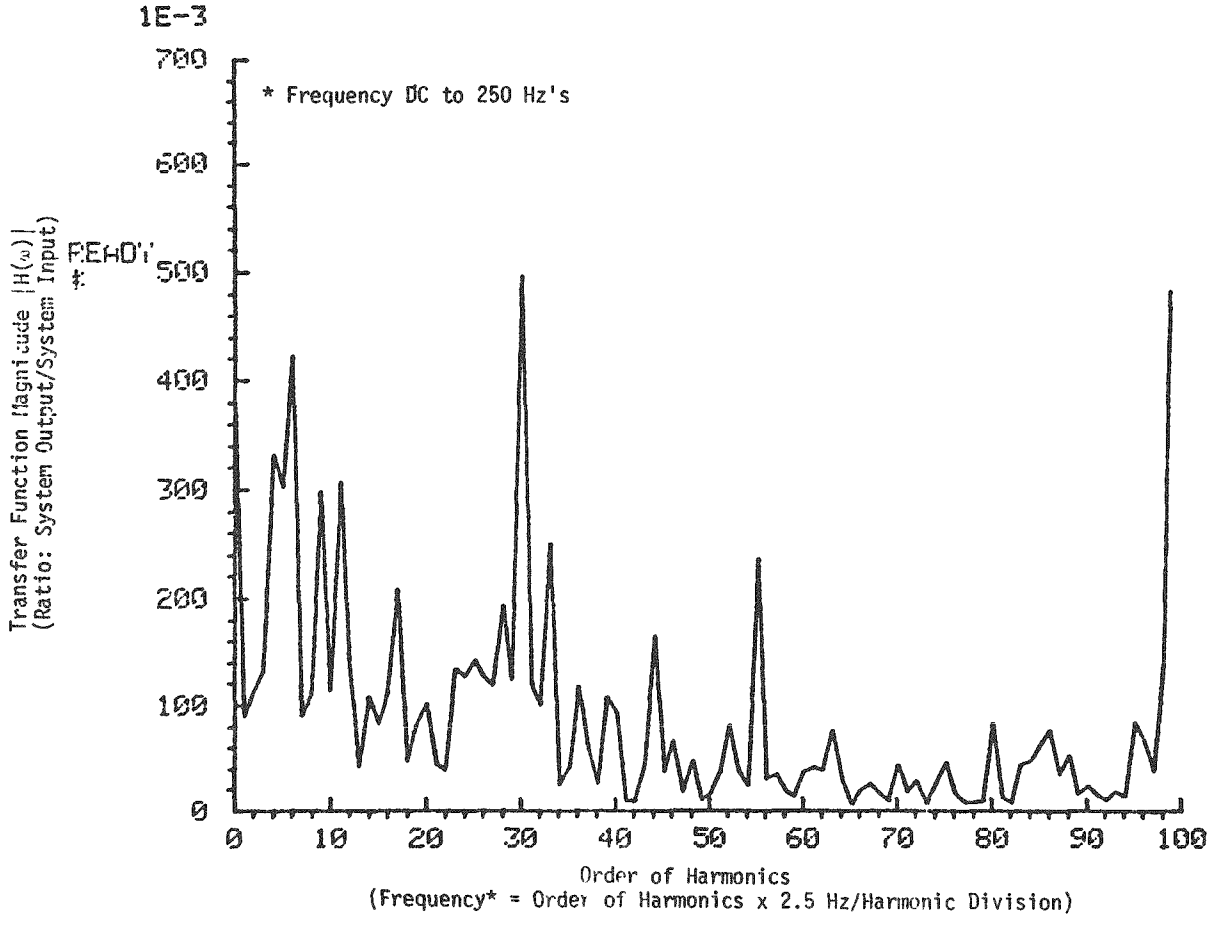

FIGURE 26. Transfer Function Magnitude vs Frequency (Vertical Energy Transfer from Instrument No. 22 to Instrument No. 11).

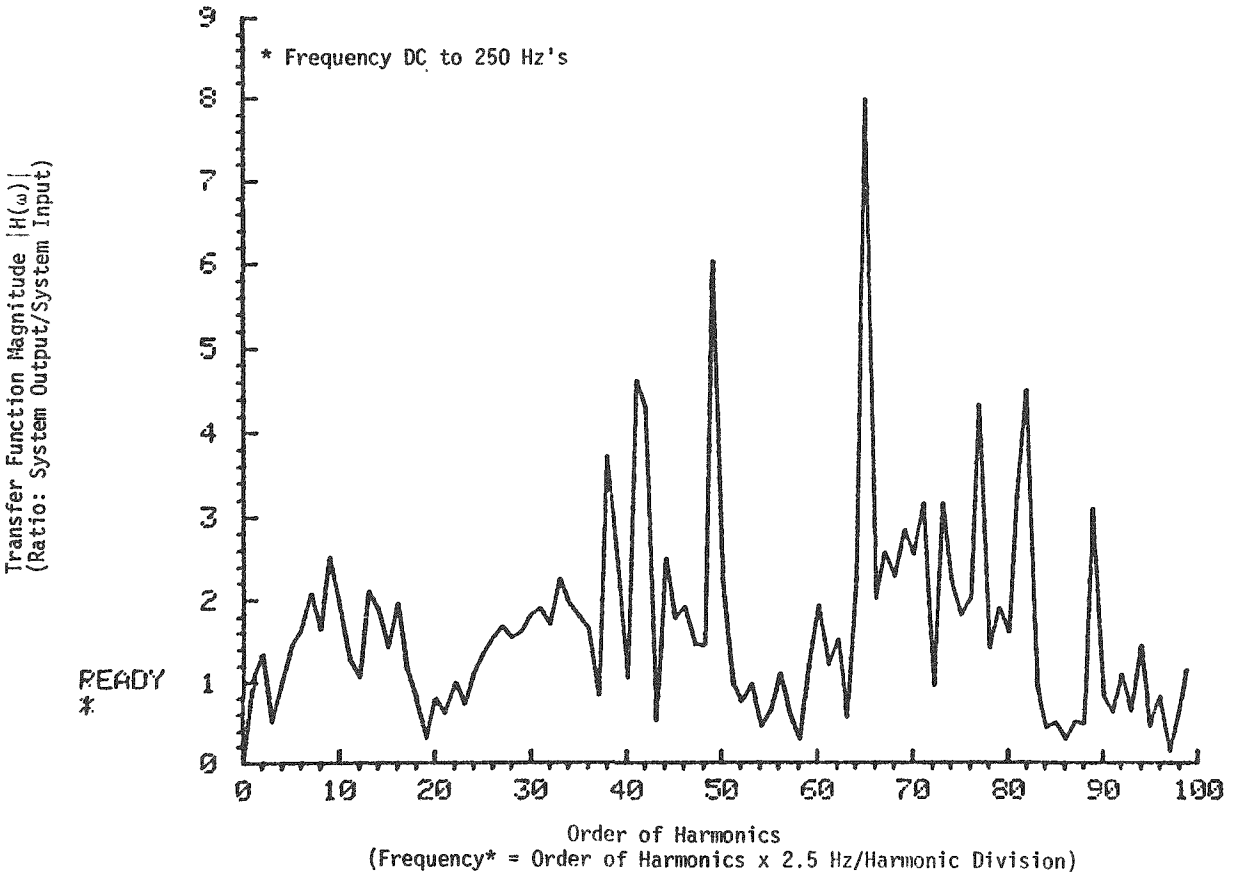

FIGURE 27. Transfer Function Magnitude vs Frequency (Vertical Energy Transfer from Instrument No. 11 to Instrument No. 9).

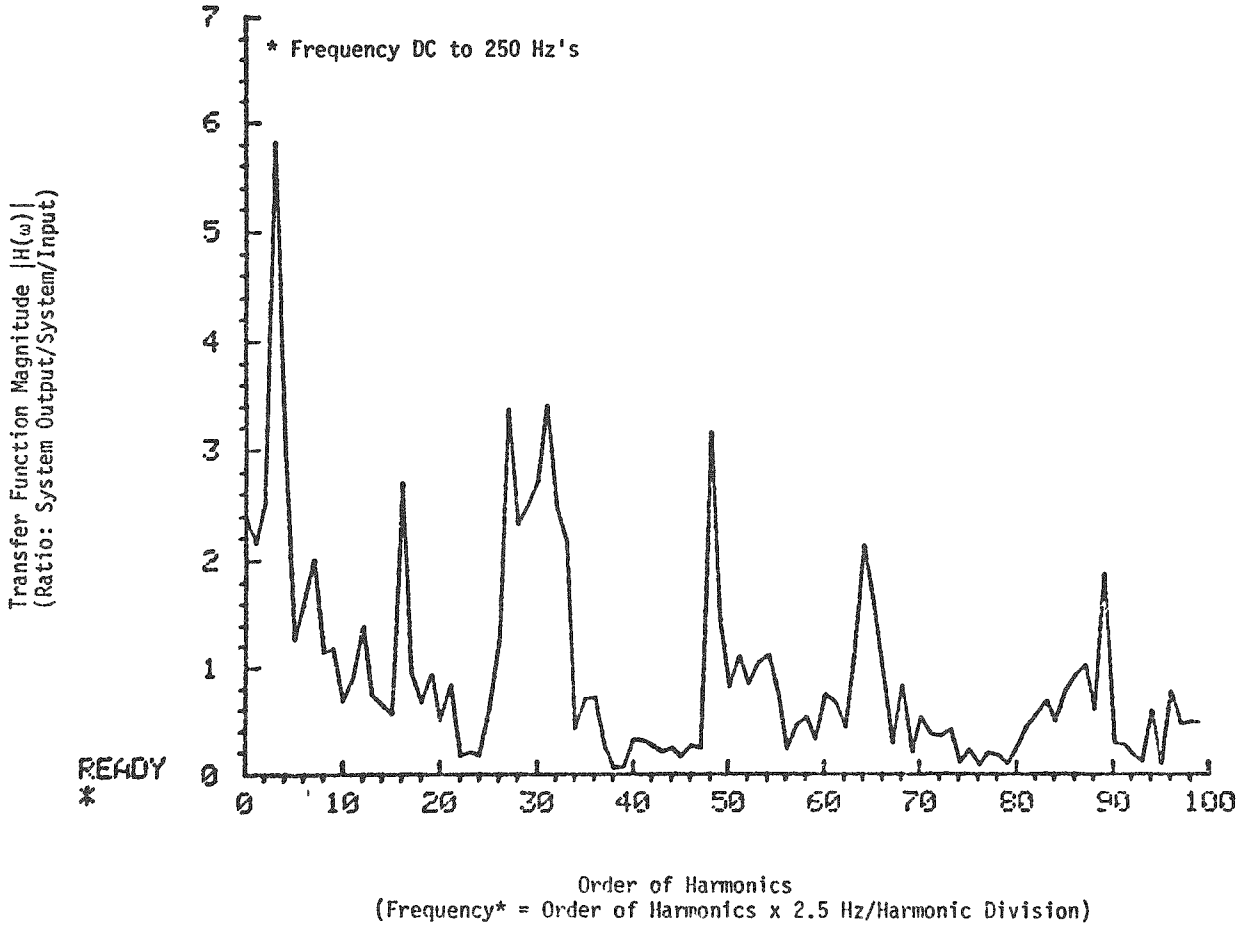

FIGURE 28. Transfer Function Magnitude vs Frequency (Horizontal Energy Transfer from Instrument No. 12 to Instrument No. 10).

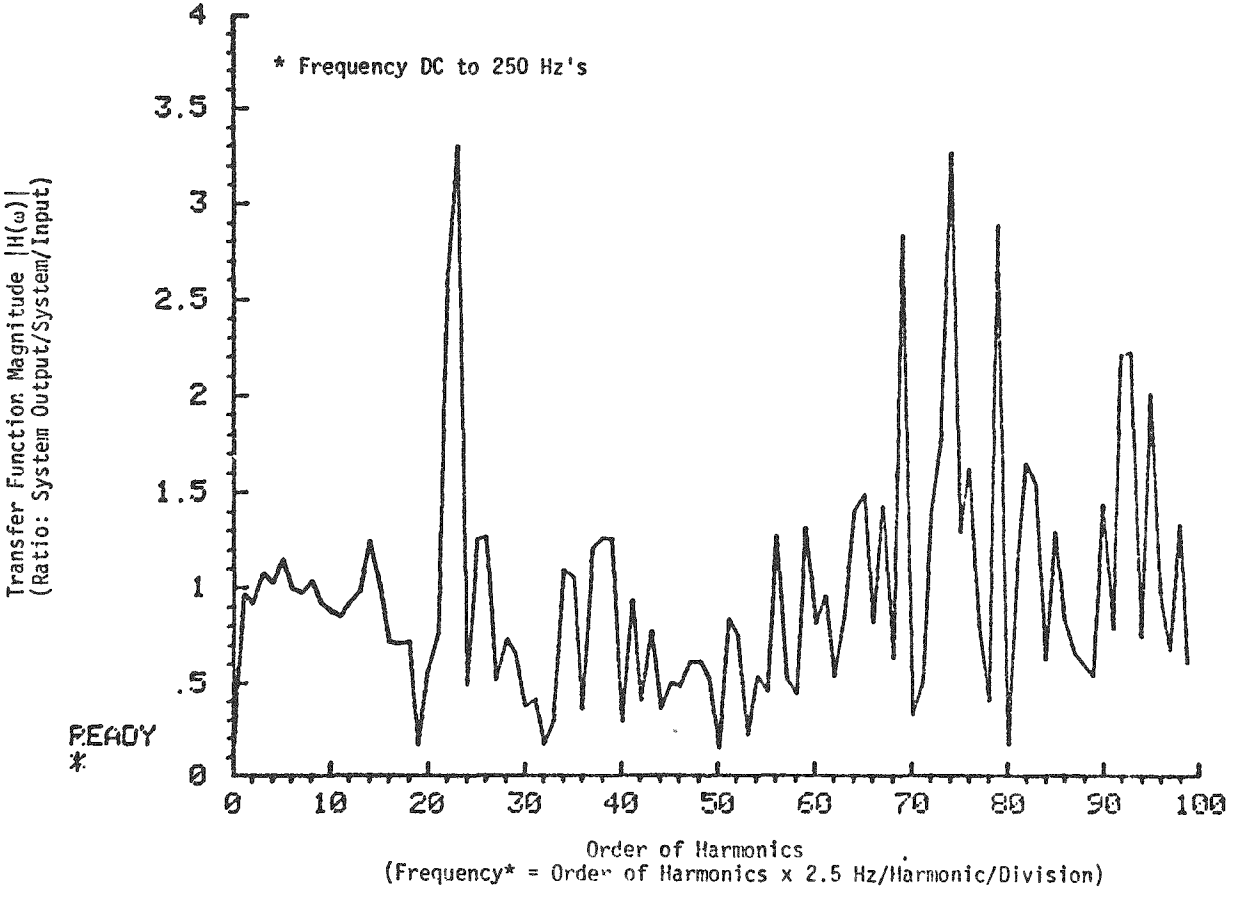

FIGURE 29. Transfer Function Magnitude vs Frequency (Horizontal Energy Transfer from Instrument No. 10 to Instrument No. 8).

F. INTERIM REPORT (TASK 6)

No interim reports were prepared during this reporting period.

G. FINAL REPORT (TASK 7)

This report has been rescheduled for completion at a later date.

IV. REFERENCES

1. S. R. Fields and S. J. Mech, Dynamic Analysis to Establish Normal Shock and Vibration of Radioactive Material Shipping Packages, NUREG/CR-0589 (HEDL-TME 78-102), Fourth Quarterly Progress Report (July 1, 1978 - September 30, 1978), November 1978.

2. C. L. Combes, et al, 1966 Car and Locomotive Cyclopedia, 1st Edition, Simmons-Boardman Publishing Corporation, New York, NY, 1966.

3. S. R. Fields and S. J. Mech, Dynamic Analysis to Establish Normal Shock and Vibration Environments Experienced by Radioactive Material Shipping Packages, NUREG/CR-0161 (HEDL-TME 78-41), Second Quarterly Progress Report (January 1, 1978 - March 31, 1978), July 1978.

4. R. W. Ramirez, The FFT: Fundamentals and Concepts, Tektronix, Inc., P. O. Box 500, Beaverton, OR, 1975.

5. A. Papoulis, The Fourier Integral and Its Application, McGraw-Hill, New York, NY, p. 27, 1962.

DISTRIBUTION

DOE/Richland Operations (4)
P. O. Box 550
Richland, WA 99352

Chief Patent Attorney
B. J. Melton
J. D. White (2)

DOE/FFTF Project Office
P. O. Box 550
Richland, WA 99352

Director

DOE Chicago Patent Office
9800 S. Cass Avenue
Argonne, IL 60439

A. A. Churm

DOE Environmental Control and Technology Division
Washington, DC 20545

J. Counts

Hanford Engineering Development Laboratory (35)
P. O. Box 1970
Richland, WA 99352

Supervisor, Document Processing W/C-123

Los Alamos Scientific Laboratory
P. O. Box 1663
Los Alamos, NM 87545

T. D. Butler

Sandia Laboratories
P.O. Box 5800
Albuquerque, NM 87115

C. F. Magnuson

Pacific Northwest Laboratory
P. O. Box 999
Richland, WA 99352

L. D. Williams

E. I. DuPont de Nemours and Company
P. O. Box A
Aiken, SC 29801

S. F. Petry